APPLICATION OF COINCIDENCE ION MASS SPECTROMETRY FOR CHEMICAL AND STRUCTURAL ANALYSIS AT THE SUB-MICRON SCALE

A Thesis

by

SARA BALDERAS

Submitted to the Office of Graduate Studies of
Texas A&M University
in partial fulfillment of the requirements for the degree of

MASTER OF SCIENCE

August 2005

Major Subject: Chemistry

APPLICATION OF COINCIDENCE ION MASS SPECTROMETRY FOR CHEMICAL AND STRUCTURAL ANALYSIS AT THE SUB-MICRON SCALE

A Thesis

by

SARA BALDERAS

Submitted to the Office of Graduate Studies of
Texas A&M University
in partial fulfillment of the requirements for the degree of

MASTER OF SCIENCE

Approved by:

Chair of Committee,	Emile A. Schweikert
Committee Member,	W. Dennis James
	Gyula Vigh
Head of Department,	Emile A. Schweikert

August 2005

Major Subject: Chemistry

ABSTRACT

Application of Coincidence Ion Mass Spectrometry for Chemical and Structural Analysis at the Sub-Micron Scale. (August 2005)

Sara Balderas, B.S., Texas A&M University

Chair of Advisory Committee: Dr. Emile A. Schweikert

Surfaces can be probed with a variant of secondary ion mass spectrometry (SIMS) where the bombardment is with a sequence of single keV projectiles, each resolved in time and space, coupled with the separate record of the secondary ions (SIs) ejected from each projectile impact. The goal of this study was to demonstrate an efficient mode of SIMS where one obtains valid analytical information with a minimum of projectiles and hence a minimum of sample consumption. An inspection of the ejected SIs from individual bombardment events will reveal "super efficient" collision cascades i.e., events, where two or more secondary ions were emitted simultaneously. It has been shown that these coincidental emissions can provide information about the chemical composition of nano-domains.

Previous studies using coincidence counting mass spectrometry (CCMS) indicated an enhancement of identifying correlations between SIs which share a common origin. This variant of SIMS requires an individual projectile impact thus causing SI emission from a surface area of ~5 nm in radius. Thus, in an event where two or more

SIs are ejected from a single projectile impact, they must originate from atoms and molecules co-located within the same nano-domain.

Au nanorods covered by a 16-mercaptohexadecanoic acid (MHDA) monolayer were analyzed using this methodology. A coincidence ion mass spectrum was obtained for the MHDA monolayer covered Au nanorods which yielded a peak for a Au adduct. Similar results were obtained for a sample with a MHDA monolayer on a Au coated Si wafer.

A series of samples consisting of Cu aggregates and AuCu alloys were investigated by SIMS to demonstrate that this technique is appropriate for characterizing nanoparticles. The mass spectra of these samples indicated that Au_{200}^{4+} is an effective projectile to investigate the surface of the target because it was able to penetrate through the poly(vinylpyrrolidone) (PVP) stabilizer that coated the surface of these nanoparticles. Coincidence mass spectra of the Cu aggregates yielded molecules co-located within the same nano-domain.

Finally, this methodology was used to investigate surface structural effects on the occurrence of "super-efficient" events. The results indicated that it is possible to distinguish between two phases of α-ZrP compounds although the stoichiometry remains the same.

DEDICATION

To

the members of my family that believed in me,

especially Bill, Vicky, and George (&).

ACKNOWLEDGEMENTS

I would like to begin by thanking Dr. E. A. Schweikert, my advisor, for his guidance and patience. Thanks to members of the Center for Chemical Characterization. Dr. Dennis James thanks for all your help with the ICP-MS. Mike Raulerson thanks for always asking, "How's it going spud?" Charlene Helton, thank you for your endless help! If I ever come across and empty transparency tray, I'll smile and think of you.

I'm also thankful to my group members. Dr. Stan Verkhoturov, thank you for your guidance in my research throughout the past few years. It is greatly appreciated. Dr. Rick Rickman, thanks for keeping my belly filled with delicious smoked brisket and sausages. I will always cherish your Saturday evening smoke outs with Linda, Jake, Zack and Claire. Jay Locklear, thanks for all the health nut comments you made. Surely, someday I'm bound to make it back to the gym. Zhen Li it has been a pleasure sharing an office with you. Thanks for always being willing to help George move my numerous boxes all around College Station. I'm sure one day I'll learn to live in one location for longer than six months. Dr. Christelle Guillermier a.k.a., Nano Christelle, thanks for all the help you have given me. I have truly enjoyed getting to know you. You are just amazing! Veronica Pinnick, thanks for all the discussions on 'weird' guy and all other banter.

To my friends in and out of the department, thank you for everything. To my Dutch, thanks for always being happy to see me. Edith Osborne thanks for taking me on outings. Our trip to Independence, Brenham, and Caldwell will be one I remember for a

long time. I will treasure the times I spent packing, shopping (with my daughter at SAMs), laughing, and stampin' with Chiquita Banana. May your life be filled with glitter! Linda Rickman, thanks for introducing me to a world outside of Chemistry. I'm not sure how much I remember from your crash course in sewing but thanks anyway. I hope your stampin' fairy visits you often. To my former roommate, Leticia Espinosa, thanks for always listening to my innumerable grievances over my failing projects and general chemistry lab stuff. You have always given me great advice. To my second former roommate, Ann Hwang, you have accomplished the impossible. You made me care about my skin! I feel like such a girly-girl! Thanks for the late night chit chats we had. To my future life long roommate, the best thing about grad school, thanks for your love, patience, support and understanding. I'm grateful that you convinced me to give 'us' a try. You truly make me happy. Rover!

TABLE OF CONTENTS

CHAPTER Page

LIST OF FIGURES

FIGURE Page

LIST OF TABLES

CHAPTER I

INTRODUCTION

There are numerous analytical techniques for analyzing solid surfaces. One such versatile technique is secondary ion mass spectrometry (SIMS). The identification of the secondary ions (SIs) sputtered from the surface via this desorption/ionization method of mass spectrometry is based on the bombardment of solid surfaces with 5-50 keV ions. SIMS can identify isotopes as well as molecular species. The success of the technique is documented with an abundance of literature [1-6].

In SIMS, the surface is bombarded with a beam of projectiles either in a static mode (usually of 10^5 -10^{12} projectiles/cm^2) or in a dynamic mode where the fluence of projectiles is such that molecules are sputtered off which in turn is used to obtain depth profiles of analytes. The flip side of this approach is that the sample is destroyed as it is analyzed. In the present strategy, we have used a "super static bombardment" approach which will not allow depth profiling but minimizes sample damage. We intend to demonstrate an efficient mode of SIMS where one obtains valid analytical information with a minimum of projectiles and hence a minimum of sample consumption. Efforts in this direction are needed to make SIMS amenable to nano-domain analysis.

Another surface analysis technique that successfully identifies SIs sputtered from solid surfaces is Cf^{252} plasma desorption mass spectrometry (PDMS). In PDMS, SIs are

---

This dissertation follows the style and format of *Journal of Mass Spectrometry*.

desorbed from a solid surface by the impact of a ^{252}Cf fission fragments [7,8]. PDMS is suitable as surface sensitive technique because the depth of a solid being probed, using this technique, is in the range of 3-300 Å [9,10].

Previous studies using Coincidence Counting Mass Spectrometry (CCMS) indicate an enhancement of identifying correlations between SIs which share a common origin [11-15]. This variant of SIMS focuses on an individual projectile impact that causes SI emission from a surface area of ~5 nm in radius [8]. Thus, in an event where two or more SIs are ejected from a single projectile impact, they must originate from atoms and molecules co-located within the same nano-domain. In this study, total matrix of events (TME) data acquisition software stores all events, i.e. all secondary ions detected from each primary impact. This software makes it possible to extract events where coincidental ion emissions occur. It has been shown that these coincidental emissions can provide information about the chemical composition of nano-domains [16, 17]. There have also been some indications that the composition and abundance of the coincidence SIs may reflect the structural arrangement in the nano-volume probed [18]. This research focuses on:

a) the validation of nano-domain chemical analysis via CCMS;
b) the relationship between the type and abundance of SIs, and structure of ionic and molecular species in the surface layers from which they originate.

The test case for nano-domain characterization will be Au nanorods and AuCu nanocrystals, while the test case for structural information will be α-Zirconium bis(monohydrogen orthophosphate) monohydrate (α-ZrP).

Nanorods

Nano-particles are of interest in bio-analysis, molecular electronics, and "bar-coding" dyes [19-21]. Natan and Keating have developed a method to produce cylindrically shaped metal nanorods with various, alternating striping patterns [19]. Previously, these unique striping patterns have been analyzed by electron and optical microscopy [20]. Transmission electron microscopy (TEM) has been used to measure the dimensions of barcodes.

Various striping patterns allow nanorods to be derivatized with several molecules by self-assembly. Barcodes consisting of Au and Pt can be derivatized with thiol and isocyanide self-assembled monolayers, respectively. The orthogonally derivatized barcodes have been characterized by fluorescence [21]. However, the fluorescence signal have been interpreted based on the excitation/emission wavelengths of the fluorescence dyes used. Our research applies a more definitive technique, specifically coincidence ion mass spectrometry.

Previously, our research group has investigated 'bare' Au/Pt and Au/Pt nanorods covered with a self-assembled monolayer (SAM) with coincidence ion measurements via plasma desorption mass spectrometry (PDMS). In that study, the PDMS spectrum of non-coated Au/Pt nanorods has failed to reveal peaks associated with Pt and Au. Peaks ranging from m/z 246 to 248 have been identified as a $PtCN^-$ adduct. A peak with m/z 249 have been identified as possibly being $Au(CN)_2^-$. A coincidence spectrum of m/z 249 has suggested that a thick layer of CN^- must have covered the nanorods since Pt and Au peaks are not revealed. It is not certain from where the CN^- group originated.

Results of the SAM covered Au/Pt nanorods also failed to produce peaks for Au and Pt. Again, suggesting a layer of CN^- must have covered the nano-surfaces. However, results have also indicated that the nanorods are partially covered by the SAM. Thus, suggesting that the nanorods are not successfully derivatized. This study will focus on investigating single elemental nanorods to verify that CCMS is an effective technique for nano analysis.

Nanocrystals

Developing selective syntheses of inorganic nanocrystals has recently been spurred by an increased interest in using nanocrystalline inorganic solids as building blocks for new nanoscale devices and technologies [22]. R.E. Schaak has developed a multistep approach to synthesize atomically ordered intermetallic nanocrystals. The initial step involved forming poly(vinylpyrrolidone) (PVP) stabilized Cu and Au nanoparticles by aqueous borohydride reduction of copper acetate and gold chloride. Transmission electron microscopy (TEM) suggests that irregularly shaped aggregates are formed [23]. Powder X-ray diffraction (XRD) data revealed that when the aggregates are heated to 150 °C Cu begins to diffuse into the Au thus forming a disordered solid solution (alloy), and heating between 200 and 400 °C forms an atomically ordered AuCu structure (intermetallic nanocrystal) [23]. In this study, CCMS has be utilized to characterize the surfaces of each of these nano-domains.

α-Zirconium bis(monohydrogen orthophosphate)monohydrate (α-ZrP)

α-Zirconium phosphate (α-ZrP) has been shown to be a versatile inorganic ion exchanger. Amorphous α-ZrP gels are used in decontamination of radioactive waste water. The crystalline form of α-ZrP is used in applications such as membrane and solid electrolyte technology, chromatography, and catalysis [24].

The crystalline α-ZrP compound, a clay-like material, is prepared from a gel by refluxing in strong phosphoric acid. The degree of crystallinity depends on the concentration of phosphoric acid and the reflux time. Powder X-Ray Diffraction is used to determine the crystal structure of α-ZrP [24]. Both the amorphous and crystalline α-ZrP, have a complex unit cell structure that consists of zirconium, phosphorus, oxygen, and hydrogen atoms.

Previously, PDMS coincidence measurements used to study the emission of secondary ions from an amorphous α-ZrP and polycrystalline α-ZrP samples, indicated differences in the respective mass spectra even though both samples were stoichiometrically the same. It was shown that the formation of negative ions from the polycrystalline α-ZrP sample is by direct emission, not by fragment recombination [25]. Coincidence counting mass spectra for both the amorphous and crystalline α-ZrP samples have shown that mass clusters greater than 400amu are only present for the crystalline form. No further change in cluster ion peaks identity or intensity was observed at higher crystallinity where the order extends over more than 100 Å [26]. Therefore, results have shown that an abundance of high mass ions correlate with crystallinity. This study will investigate the relationship between the type and

abundance of SIs, and structure of ionic and molecular species in the surface layers from which they originate.

CHAPTER II

EXPERIMENTAL

Plasma Desorption Mass Spectrometry Instrumentation (PDMS)

PDMS is based on the fission fragments from the decay of ^{252}Cf radioisotope. This source can undergo spontaneous fission emission of fast heavy ions in the mass range of 95-160 Daltons and with the energy of 60-120 MeV [9, 10]. Two complementary fission fragments are produced during a fission event. They traveled at approximately 180° from each other.

When a fission fragment struck the electron conversion foil positioned directly in front of a chevron array microchannel plates (MCP), a start signal was produced (Fig. 2-1). The complimentary fission fragment hit a biased sample at a 45° angle of incidence (for AuCu experiments the incidence angle was 30°), and caused emission of secondary ions. The desorbed secondary ions were accelerated through a grounded grid and traveled in a drift region 56 cm in length. They produced stop signals at a MCP detector located at the end of the flight tube.

The output signal at the MCP was fed into the constant fraction discriminator (CFD). If the input to the CFD was above the user determined threshold, a negative five volt (NIM) square pulse was the output. This output was fed to the time-to-digital converter (TDC), where if correlated to a start signal was assigned a time bin. Each event was transferred from the TDC to the PC for storage and analysis via Total Matrix of Events (TME) software [27].

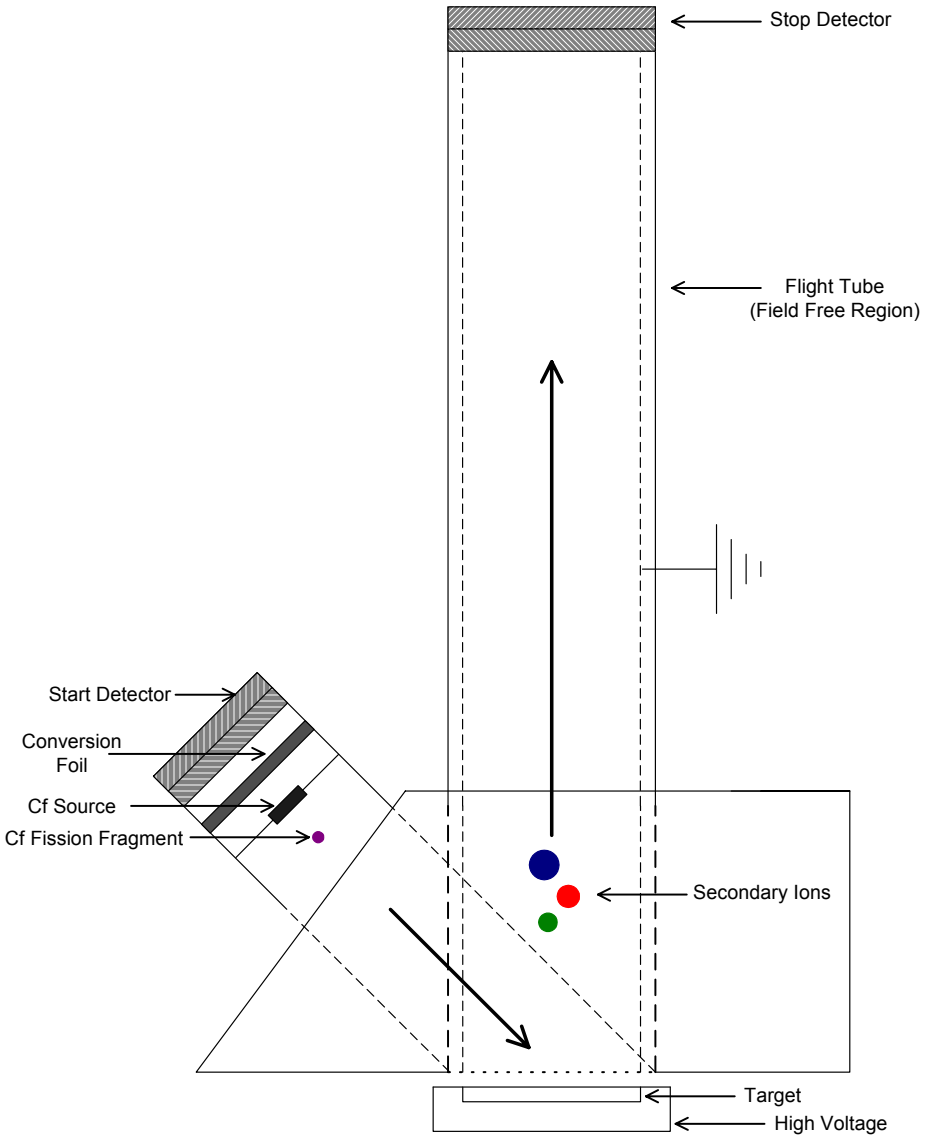

Figure 2-1. Schematic illustration of PDMS instrument. Diagram is not to scale.

Vacuum Chamber

The PDMS setup was housed in a 29cm diameter stainless steel vacuum chamber (Kurt J. Lesker,Clairton, PA). A base pressure of ~10^{-6} torr was maintained by a diffusion pump (Edwards High Vacuum, Grand Island, NY) that was backed up by a 12 cfm rotary vane mechanical pump. Chilled water (Haskris Company, Type R150, Arlington Heights, IL) with an average flow of 2-3 gal/min was used to cool the diffusion pump.

Samples were introduced into the instrument without breaking the vacuum pressure by attaching a stainless steel gate valve (MDC, Model GV-1500V, Hayword, CA) to the main chamber. The sample inlet design required a threaded linear-rotary motion feedthrough (MDC, Model K-CRPP-1). A stainless steel or brass sample cube, with dimensions of 1.5cm x 1.0cm x 1.5cm, was screwed onto the threaded end of the feedthrough rod, and attached to the sample inlet via a Quik-Flange (Duniway Stockroom Corp., Mountainview, CA). A Welch roughing pump was also attached to the sample inlet system via a brass valve (Key High Vacuum Products, Inc. Model BA-112, Nesconset, NY). The brass valve was opened to evacuate the sample inlet area for several minutes. Once the area is evacuated (< 10^{-3-} torr) the brass valve was closed and the stainless steel gate valve on the main chamber was opened. The threaded rod was inserted into the main chamber, the sample cube was inserted into a Teflon sample holder, the threaded rod was unscrewed and withdrawn from the main chamber, and the stainless steel gate valve was closed to reestablish vacuum pressure.

Time-of-Flight Mass Analysis

Time of flight analysis was used in the experiments discussed herein for identification of desorbed secondary ions. In these experiments, from the time an ion was desorbed from the sample surface until it was detected, the ion experienced at least two distinct regions that affected its recorded flight time. The regions were the acceleration, and field-free drift regions. The summation of the flight times of these regions was:

$$T_{tot} = t_a + t_d \qquad \text{Eq. 2-1}$$

where t_a and t_d were the flight times, in seconds, for the ion in the acceleration and field-free drift region, respectively.

The time it took the ion to travel through the acceleration region, t_a, was given by:

$$t_a = \sqrt{\frac{2 L_a^2}{V}} \sqrt{\frac{m}{q}} \qquad \text{Eq. 2-2}$$

where V was the voltage on the sample given in volts, L_a was the length of the acceleration region in meters, and m was the mass of the ion with charge q. Next, the ion encountered the drift field-free region. The time the ion spent in this region was given by:

$$t_d = \sqrt{\frac{L_d^2}{2V}} \sqrt{\frac{m}{q}} \qquad \text{Eq. 2-3}$$

where L_d was the length of the drift field-free region. Hence, the following expression could be obtained:

$$t_{tot} = t_a + t_d = \sqrt{2}\sqrt{\frac{m}{q}}\left(\sqrt{\frac{L_a^{\,2}}{V}} + \frac{1}{2}\sqrt{\frac{L_d^{\,2}}{V}}\right) . \qquad \text{Eq. 2-4}$$

To mass calibrate the collected spectrum the known variables L_d, L_a, V, and t_{tot} allows for the mass identification using Eq. 3-4. This entails a tedious calculation for the mass assignment of each peak. This approach is simplified by knowing that the flight time, t_{tot}, of an ion is proportional to the square root of its m/q ratio, all other factors can be reduced to two constants giving the following [31, 32]:

$$t_{tot} = \sqrt{\frac{m}{q}}C_1 + C_2 \qquad \text{Eq. 2-5}$$

The user was able to select at least two secondary ions with known masses to calculate two equations for C_1 and C_2 to calibrate the total spectrum. The spectra discussed herein were typically converted from a time scale to a mass-to-charge scale using H^+ and Na^+ in the positive mode, and H^- and C_2H^- in the negative mode.

Cluster Secondary Ion Mass Spectrometry Instrumentation

A gold liquid metal ion source (LMIS) was used to produce polyatomic projectiles such as Au_n^+ (n= 2-5) [Fig. 2-2]. An electrostatic lens was used to focus the extracted ions through a Wien filter, high voltage plates, and finally a 400μm diameter collimator. A Wien filter was used to select the preferred primary projectile. The pulse generated by the high voltage plates provided the start signal of the primary ion time-of-flight measurement and reduced the primary ion fluence. A set of steering plates was used to direct the primary ions toward the sample target, which produced secondary ion

emissions that included: ions, photons, neutrals and electrons. An MCP array detected the ejected electrons. Constant fraction discriminators convert MCP signals into NIM logic pulses, which are in turn routed to a time-to-digital converter. The data were then transferred over to a personal computer where the identity of the primary ion was verified. The NIM logic pulse was also routed to a second time-to-digital converter where it also served as the time-of-flight start signal for the secondary ions. The stop signal for the secondary ions was produced by a second MCP array located at the end of a time-of-flight tube. The flight times of the detected secondary ions were stored via Total Matrix of Events software.

Data Acquisition

TME stored each individual event in a total event array. With all events stored, it was possible (after the acquisition was complete) to explore the data set by selecting different parameters. The software could produce a total mass spectrum by selecting all events where secondary ions were detected. A coincidence spectrum was compiled for a peak of interest by selecting a minimum and maximum channel number, representing a mass range which contained the peak of interest. TME also made it possible to obtain yields based on the number of SIs detected per event.

Target Preparation

A silicon wafer was cut into $1cm^2$ pieces using a diamond scribe and ozone cleaned. After ozone cleaning, the $1cm^2$ Si wafers were rinsed with ethanol, sonicated in

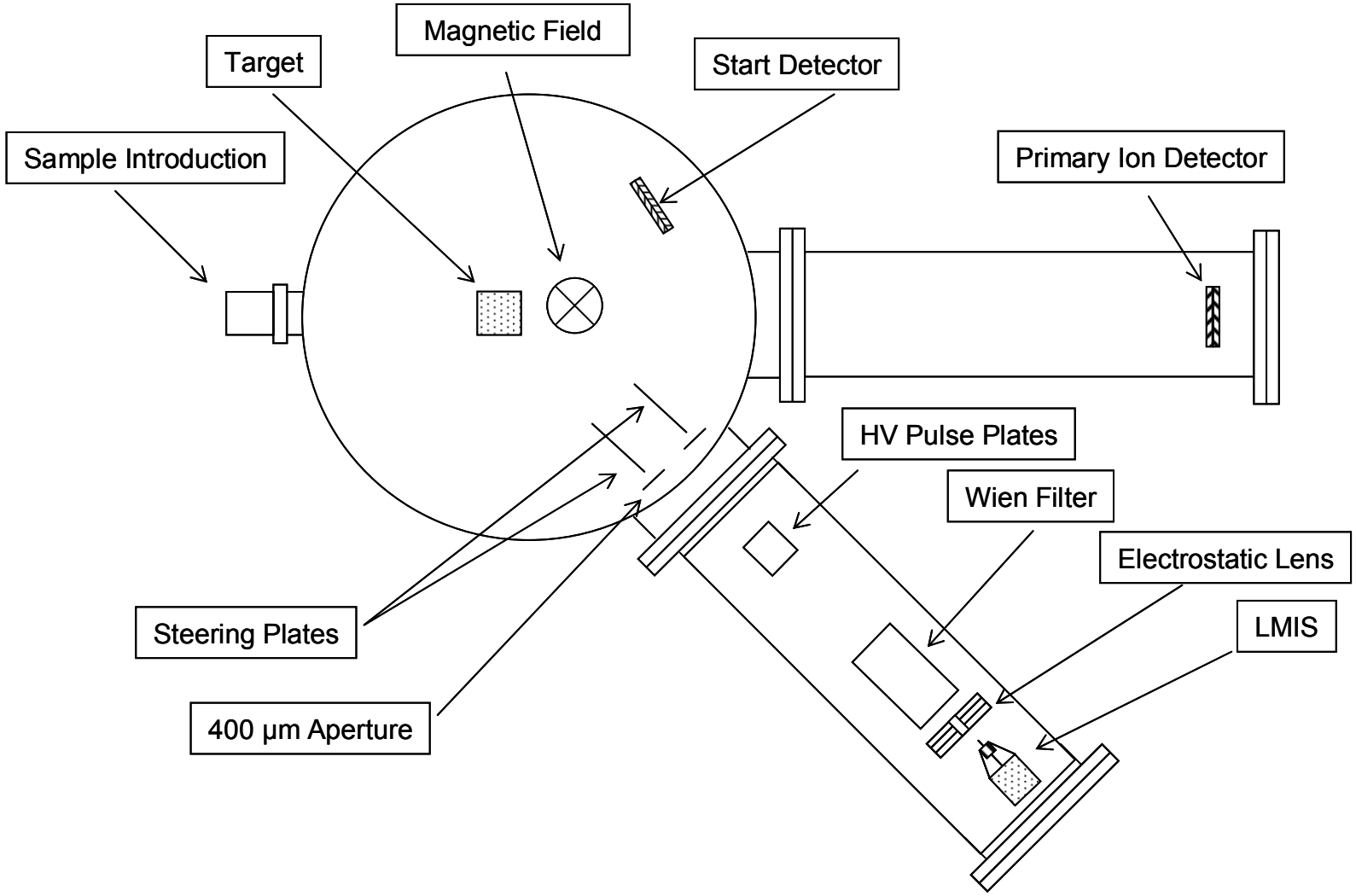

Figure 2-2. Schematic illustration of cluster SIMS instrument. Diagram is not to scale.

ethanol, rinsed again with ethanol, and dried with a stream of N_2 prior to analysis. Nanorods typically 300nm in diameter and 3μm in length were obtained from the Keating research group [19]. Approximately $2x10^9$ nanorods were suspended in 1mL of ethanol solution. The 1ml plastic micro-tube containing the nanorods and ethanol solution was sonicated for roughly one minute prior to depositing 45μl of the sample onto a $1cm^2$ silicon wafer in 5μl increments (allowing the ethanol to evaporate between each application).

The other provided sample consisting of approximately $2x10^9$ Au nanorods covered by 16-mercaptohexadecanoic acid (MHDA) suspended in 1mL of ethanol solution were deposited onto Si substrates. This sample was photooxidized for ~ 1hr using a Hg/Ar lamp. Photooxidation made it possible to easily sputter, ionize, and detect species that are characteristic of the intact monolayer molecule by converting the thiolate to a sulfonate moiety [28].

Silicon wafers coated with a 10nm Ti adhesion layer followed by a 200nm-thick layer of Au were cut into $1cm^2$ pieces using a diamond scribe. The $1cm^2$ Au coated wafers were rinsed with EtOH, ozone cleaned for 10 minutes, sonicated for 5 minutes, rinsed with EtOH and soaked in a ~0.5mM MHDA/ethanol solution for ~24hrs. After the Au coated wafers were sonicated for ~2 minutes in the MHDA/ethanol solution to remove any physisorbed material, they were removed from the solution and rinsed with ethanol and dried with a stream of nitrogen. The quality of the monolayer was tested by ellipsometry measurements. In order to determine the MHDA monolayer thickness, ellipsometry measurements were collected from 5 areas before and after the Au coated

wafer was prepared with the monolayer. The MHDA monolayer thickness was measured to be 17.9Å (± 3 Å). The sample was mounted onto a stainless steal sample cube and inserted into the desired mass spectrometer.

Silicon wafers, as described previously, were utilized as substrates for the AuCu experiments. Silicon wafers were ozone cleaned for 10mins and stored in ethanol until researchers in Schaak's group deposited 12 μl portions of roughly ~2.5M AuCu samples onto the surface of the substrate. The wafer was then mounted onto a stainless steal sample cube before the sample was mass analyzed.

The Clearfield research group provided the α-ZrP samples [24]. A small sample of α-ZrP clay was mixed with ethanol for application purposes. A slurry was made by mixing 0.05g of α-ZrP with 1mL of ethanol. Seventy-five micro-liters of the slurry were applied onto a stainless steel sample cube. Ethanol was allowed to evaporate prior to instrumental analysis.

CHAPTER III

CHARACTERIZATION OF NANORODS

As previously stated, the projectiles in coincidence ion mass spectrometry (CIMS) can be fission fragments or keV polyatomic ions. In this set of experiments, ^{252}Cf fission fragments were utilized as projectiles to confirm surface coverage of elemental nanorods in the nano-domain. The TME software was used to analyze coincidence ion emission. Since it had been shown that polyatomic projectiles such as Au_n (n = 2-5) can enhance secondary ion yields [29], Au_3^+ projectiles were selected for a comparative study of the surface composition.

SIMS

Photooxidized samples of a Si wafer, Si wafer covered by Au nanorods, and Si wafer covered by Au nanorods coated with 16-mercaptohexadecanoic acid (MHDA) were analyzed via cluster SIMS. Figure 3-1 shows the negative mass spectra produced by Au_3^+ projectiles from a (a) Si Wafer, (b) Si wafer covered by Au nanorods and (c) Si wafer covered by Au nanorods coated with MHDA. The peak at m/e 197 is thought to correspond to Au^- which is produced from the Au nanorods but this peak is also observed in the mass spectrum of the Si wafer which corresponds to $(SiO_2)_3OH^-$. The yields listed in Table 3-1 shows that the yield of m/e 197 peak in the Au nanorods sample is higher than the yield corresponding to the $(SiO_2)_3OH^-$ peak. Thus, indicating the emission of Au^- from the samples containing Au nanorods. A peak corresponding to the monolayer was observed at m/e 80 in Fig. 3-1(c). However, this fragment is also

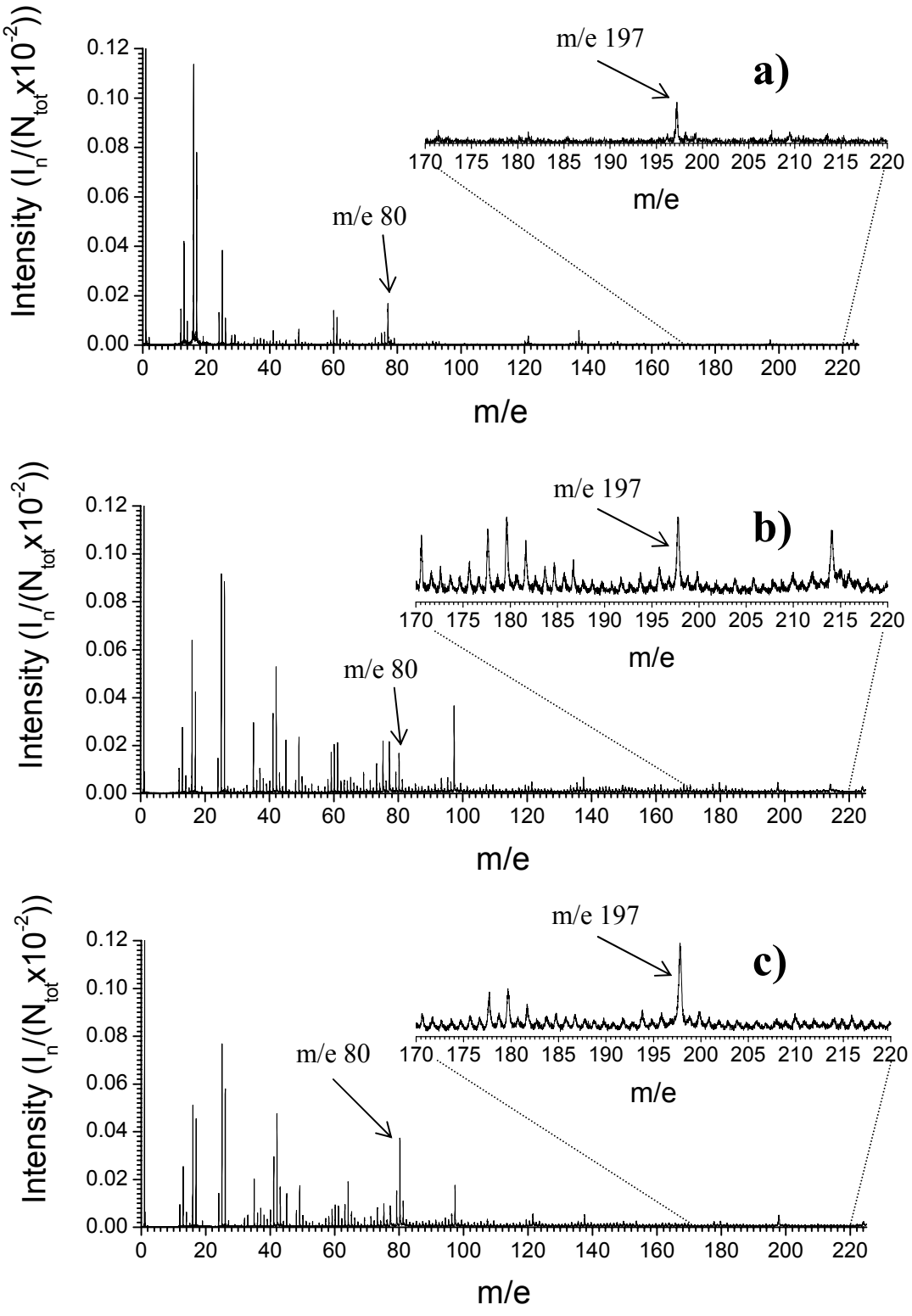

Figure 3-1. Cluster SIMS 21keV Au_3^+ mass spectra of a) Si wafer, b) Au nanorods on Si wafer, and c) Au nanorods coated with MHDA on Si wafer.

present in the mass spectrum of the Si wafer covered by the Au nanorods in Fig. 3-1(b). In Table 3-1, the yield of m/e 80 in the Au nanorod sample is higher than the yield of m/e 80 in the Au nanorod sample covered by MHDA. This is an indication that m/e 80 in Fig. 3-1(c) corresponds to SO_3^-.

A coincidence mass spectrum of the Au nanorods surface is shown on Fig. 3-2(a). The peak with m/e 80 corresponds to SO_3^-. Since the presence of the SO_3^- peak indicates the existence of thiol, this is direct evidence that the thiol monolayer exists on the Au nanorods surface. To verify this result we ran the same experiment for bare Au nanorods. Figure 3-2(b) shows the coincidence ion spectrum for emitted Au ions. There is a peak at m/e 80 which is an indication of a contamination. It can be concluded that our method can accurately check for nanorod coverage. The quality of the SAM coverage is not perfect due to the low intensity of SO_3^- peak (we had an intense SO_3^- peak in previous spectrum of SAMs on a Au coated Si wafer).

PDMS (Positive Mode)

Plasma Desorption Mass Spectrometry (PDMS) was used to investigate for positive secondary ions. With this method, MeV ^{252}Cf fission fragments bombarded the sample surface. A similar sample preparation was used, which was described in chapter II. However, the oxidation step was omitted. We investigated two nanorod samples, one covered by MHDA and the other not covered by the SAM. In the conventional mass spectrum obtained for the Au nanorods covered by MHDA [Fig. 3-3(a)], a peak at m/e 507 was identified as a thiol containing molecule, $HAuS(CH_2)_{15}COONa^+$. This adduct

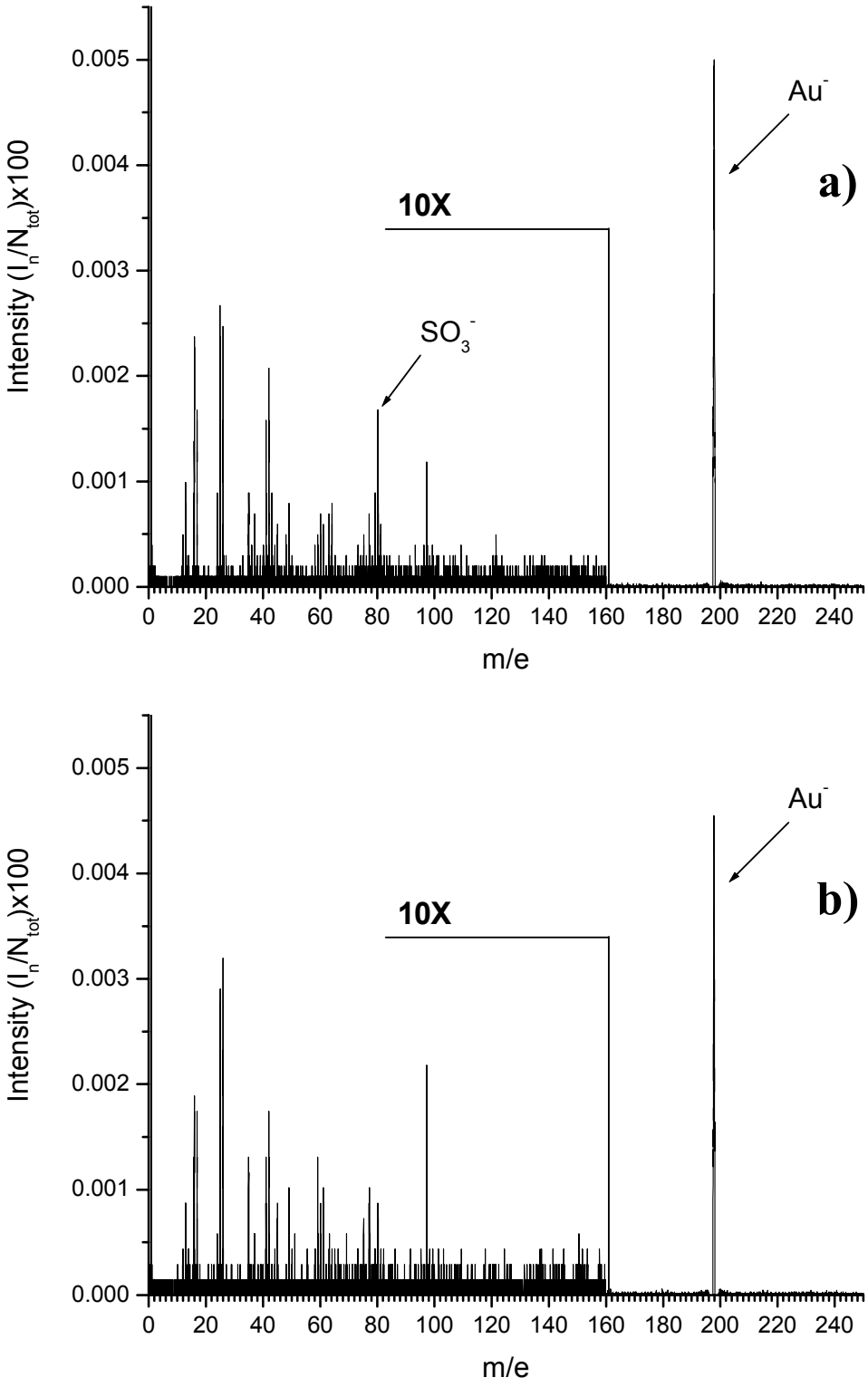

Figure 3-2. Mass spectra of ions co-emitted with m/e 197 from targets consisting of a) Au nanorods coated with MHDA on Si wafer, and b) Au nanorods on Si wafer via cluster SIMS 21keV Au_3^+.

Table 3-1. Yields for peaks with m/e 80 and 197 from negative cluster SIMS mass spectra of Si wafer, Au nanorods on Si wafer, and Au nanorods coated with MHDA on Si wafer.

	Yield		
m/e	Si Wafer	Au Nanorods	Au Nanorods with MHDA
80	7.83×10^{-5}	2.26×10^{-3}	5.12×10^{-3}
197	2.09×10^{-4}	9.13×10^{-4}	1.50×10^{-3}

occured because carboxylic acids generate a high-energy surface which contaminated rapidly in the laboratory atmosphere. A peak at m/e 23 indicated a high intensity for the Na^+. To verify that the peak at m/e 507 was an adduct for the MHDA monolayer, a Au coated Si wafer soaked in ~0.5mM MHDA/ethanol solution for ~18hrs was also analyzed via PDMS in the positive mode. Figure 3-3(b) also contained peaks at m/e 23 and 507. The conventional mass spectrum for the uncovered nanorods [Fig. 3-3(c)] yielded a low intensity peak for the Na^+ fragment. That mass spectrum also indicated the absence of the m/e 507 peak.

To verify that the sodium is arranged on the surface of Au nanorods coated with MHDA but not the surface of silicon we obtained a coincidence mass spectrum [Fig. 3-4(a)] which shows the Au adduct molecule, $HAuS(CH_2)_{15}COONa^+$, co-emitted with Na^+. Similar results were also obtained for the Au covered Si wafer coated with MHDA. The coincidental ions co-emitted with m/e 23 also revealed the existence of a peak at m/e 507 [Fig. 3-4(b)]. A coincidence spectrum was obtained for a Si wafer covered with

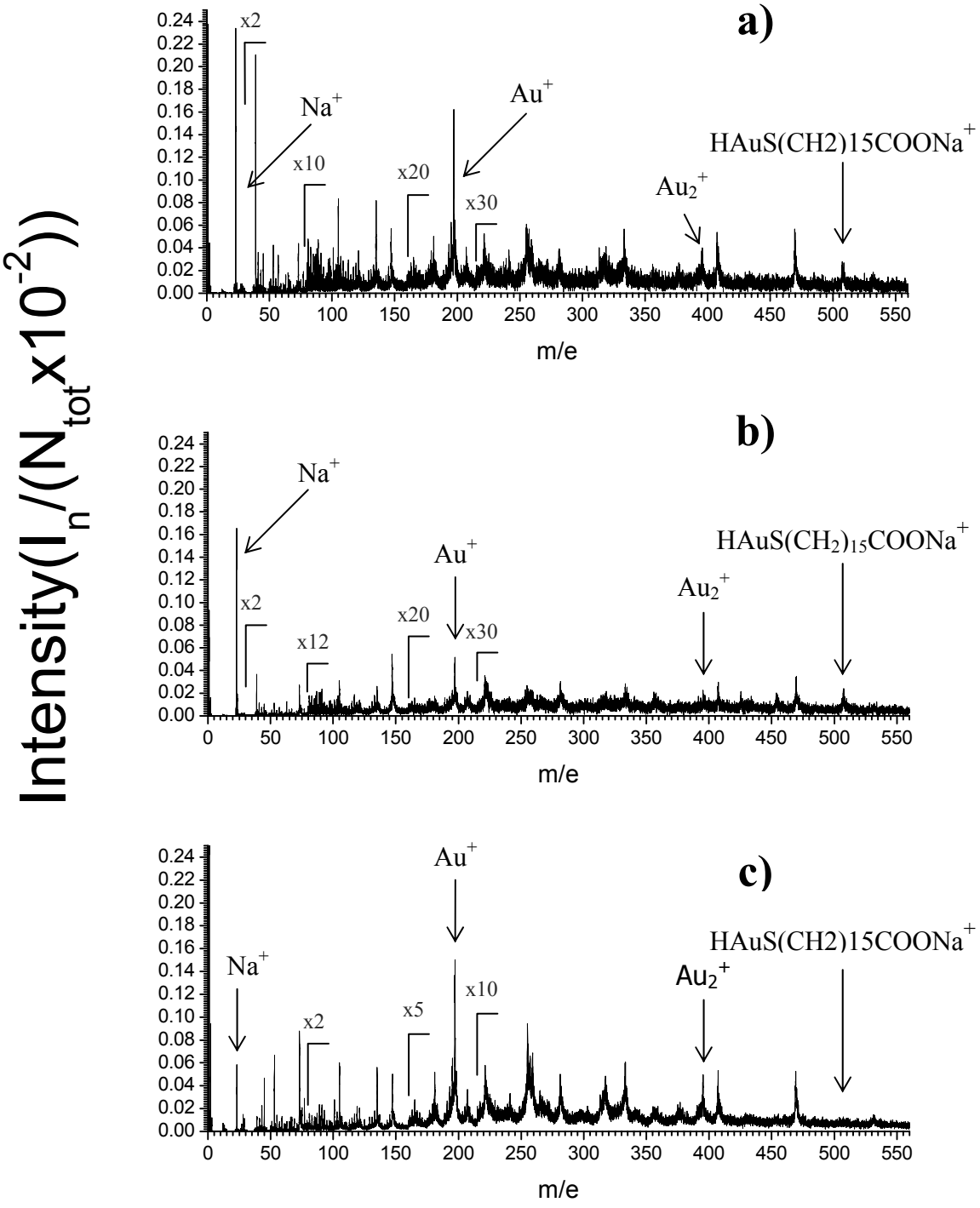

Figure 3-3. Positive PDMS mass spectrum of a) Au nanorods coated with MHDA on Si wafer, b) Au coated Si wafer coated with MHDA, and c) Au nanorods on Si wafer.

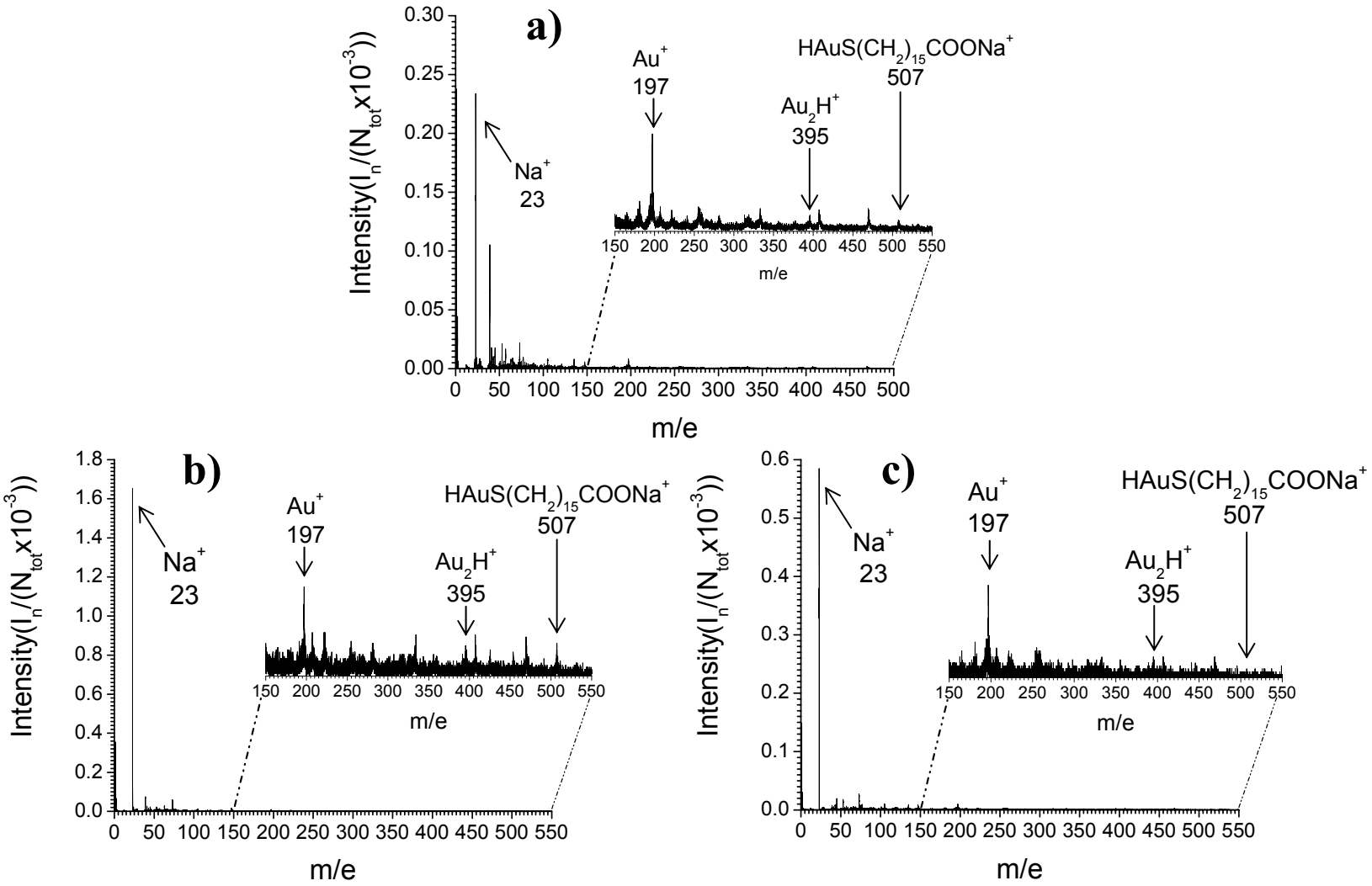

Figure 3-4. Mass spectra of ions co-emitted with m/e 23 via PDMS from targets consisting of a) Au nanorods coated with MHDA on Si wafer, b) Au coated Si wafer with MHDA, and c) Au nanorods on Si wafer.

Au nanorods [Fig. 3-4(c)]. A prominent peak for m/e 507 was not observed in the spectrum obtained of the Au coated Si substrate. These results confirm that the peak with m/e 507 results from the presence of the MHDA monolayer.

PDMS (Negative Mode)

A total mass spectrum of ions emitted for the blank Si wafer did not indicate the presence of SH^- on the substrate surface. The intensity ratio of peaks OH^- and SH^- were calculated and listed in Table 3-2 for each of the samples. When the ratio decreases, this indicates the increased intensity for the presence of SH^-. By comparing the values, this may indicate that the $HCO_2(CH_2)_{15}S^-$ monolayer is bonded to the Au nanorods. The coincidence mass spectrum of ions co-emitted with SH^- for the blank Si wafer reveals only a few contamination peaks. The coincidence spectra for the Au nanorods covered by the monolayer contained more mass peaks due to molecular fragments. This could be due not only to the presence of contamination but they could correspond to fragments from the monolayer. However, this is not conclusive considering that the molecular ion peak was not detected.

Table 3-2. Peak intensities of OH^- to SH^- fragment and ion ratios for Si wafer and nanorod samples by fission fragment bombardment.

	Peak Intensities		
	m/e		m/e Ratios
	17	33	17/33
Fragment	OH^-	SH^-	OH^-/SH^-
Si Wafer	0.00356	0.00047	7.57234
Au Nanords	0.0046	0.0018	2.55389
Au Nanorods with MHDA	0.00477	0.00451	1.05878
Oxidized Au Nanorods	0.00582	0.00197	2.95785
Oxidized Au Nanorods with MHDA	0.00445	0.00284	1.56962

CHAPTER IV

COINCIDENCE ION MASS SPECTROMETRY OF AuCu NANOPARTICLES

As discussed in the previous chapter, utilization of coincidence ion mass spectrometry provides chemical information about nano-objects within a few nanometers in diameter. The focus of the next set of experiments was to determine if CIMS is an effective analysis method for bimetallic nanoparticles. The objective was to analyze each of the steps in the synthesis of atomically ordered nanocrystals from bimetallic nanoparticles. As previously mentioned, poly(vinylepyrrolidone) stabilized Cu and Au nanoparticles are formed by the aqueous borohydride reduction of $Cu(C_2H_3O_2)_2$ and $HAuCl_4 \cdot 3H_2O$. Diffusion of Cu into Au occurs when the AuCu aggregates are collected and dried at temperatures below 175 °C, thus forming disordered alloy nanoparticles. Nucleation of atomically ordered AuCu nanocrystals occurs when the nanoparticles are annealed at 200 °C [23].

SIMS

Previous experiments have revealed that secondary ion yields increase in a supra-linear response as the complexity and velocity of the projectile increases [30]. Figure 4-1 is a plot of the yields of phenylalanine $[M-H]^-$ as a function of projectile energy per

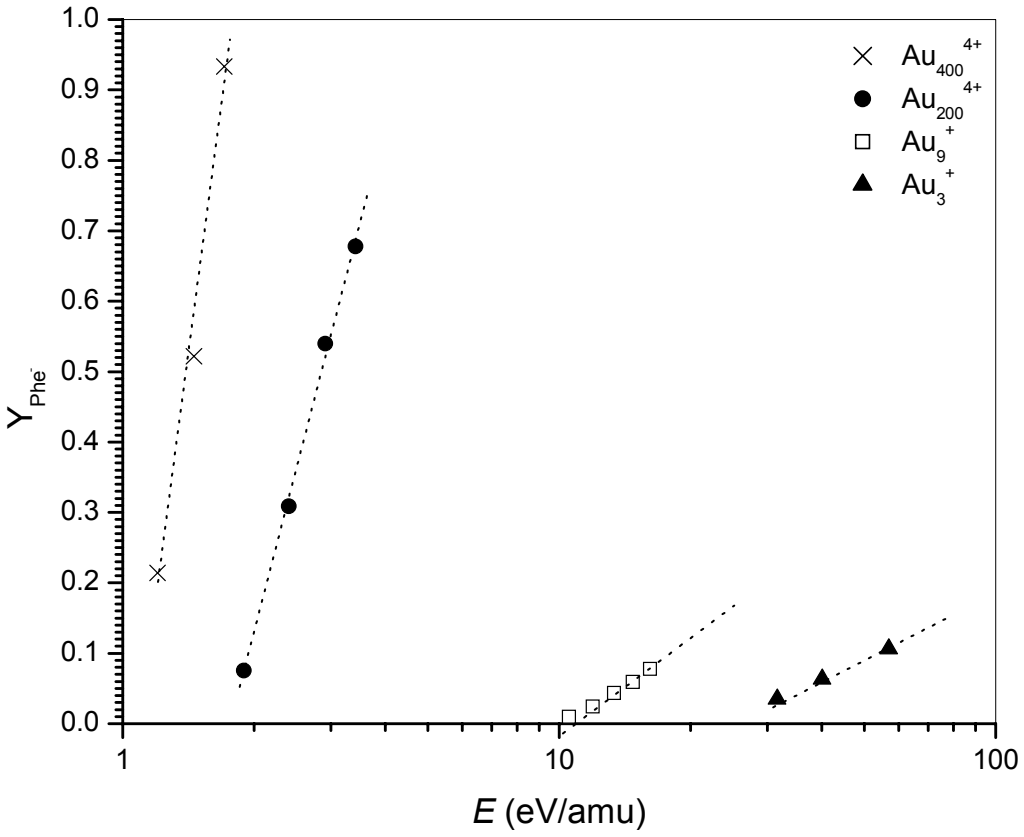

Figure 4-1. Secondary ion yields for the Phe molecular ion $(M-H)^-$ on a per atom basis as a function of the energy per atom of the Au_n^{m+} projectiles, n=3, 9, 200, 400; m=1, 4. Lines are a guide for the eye.

atom. There is a notable enhancement in secondary ion yields due to the number of constituent atoms in the projectile. For this reason, the targets in this set of experiments were bombarded with Au_{200}^{4+}. Figure 4-2 shows a mass spectrum of Cu aggregates sample. The predominant peaks resulting from the Cu aggregates sample are CNO^- (m/e 42), $C_2H_3O^-$ (m/e 43), $C_2(CNO)_2^-$ (m/e 108), $C_2(CNO)(C_2H_3O)^-$ (m/e 109), $^{63}Cu(CNO)(C_2H_3O)^-$ (m/e 148), $^{63}Cu(C_2H_3O)_2^-$ (m/e 149), $^{65}Cu(CNO)(C_2H_3O)^-$ (m/e 150), and $^{65}Cu(C_2H_3O)_2^-$ (m/e 151). Coincidental ion spectra for all ions co-emitted with m/e 43, 148, 151, and 197 are presented in Fig. 4-3. Figure 4-3(a) is a coincidence mass spectrum of all ions co-emitted with $C_2H_3O^-$ (m/e 43) which is a fragment from the PVP. The most predominant peaks are $C_2(CNO)_2^-$ (m/e 108), $C_2(CNO)(C_2H_3O)^-$ (m/e 109), $^{63}Cu(CNO)(C_2H_3O)^-$ (m/e 148), $^{63}Cu(C_2H_3O)_2^-$ (m/e 149), $^{65}Cu(CNO)(C_2H_3O)^-$ (m/e 150), and $^{65}Cu(C_2H_3O)_2^-$ (m/e 151). The peak areas for these peaks were obtained and compared to the values determined from the total mass spectrum of Cu aggregates sample (Table 4-1). The difference between the spectra is that the intensities of the peaks are higher in Fig. 4-2 thus an indication that PVP coats the entire surface. The observed ratios listed in Table 4-2 were obtained to determine if the peak area ratios of $^{65}Cu(CNO)(C_2H_3O)^-$ to $^{63}Cu(CNO)(C_2H_3O)^-$ and $^{65}Cu(C_2H_3O)_2^-$ to $^{63}Cu(C_2H_3O)_2^-$ peaks were correctly identified as copper containing fragments by comparing those ratios to that of the known isotopic ratio of ^{65}Cu to ^{63}Cu. The results indicate that this method would be able to detect copper containing fragments.

Figures 4-3(b) and 4-3(c) are coincidence mass spectra of all ions co-emitted with $^{63}Cu(C_2H_3O)_2^-$ (m/e 149) and $^{65}Cu(C_2H_3O)_2^-$ (m/e 151), respectively. The most

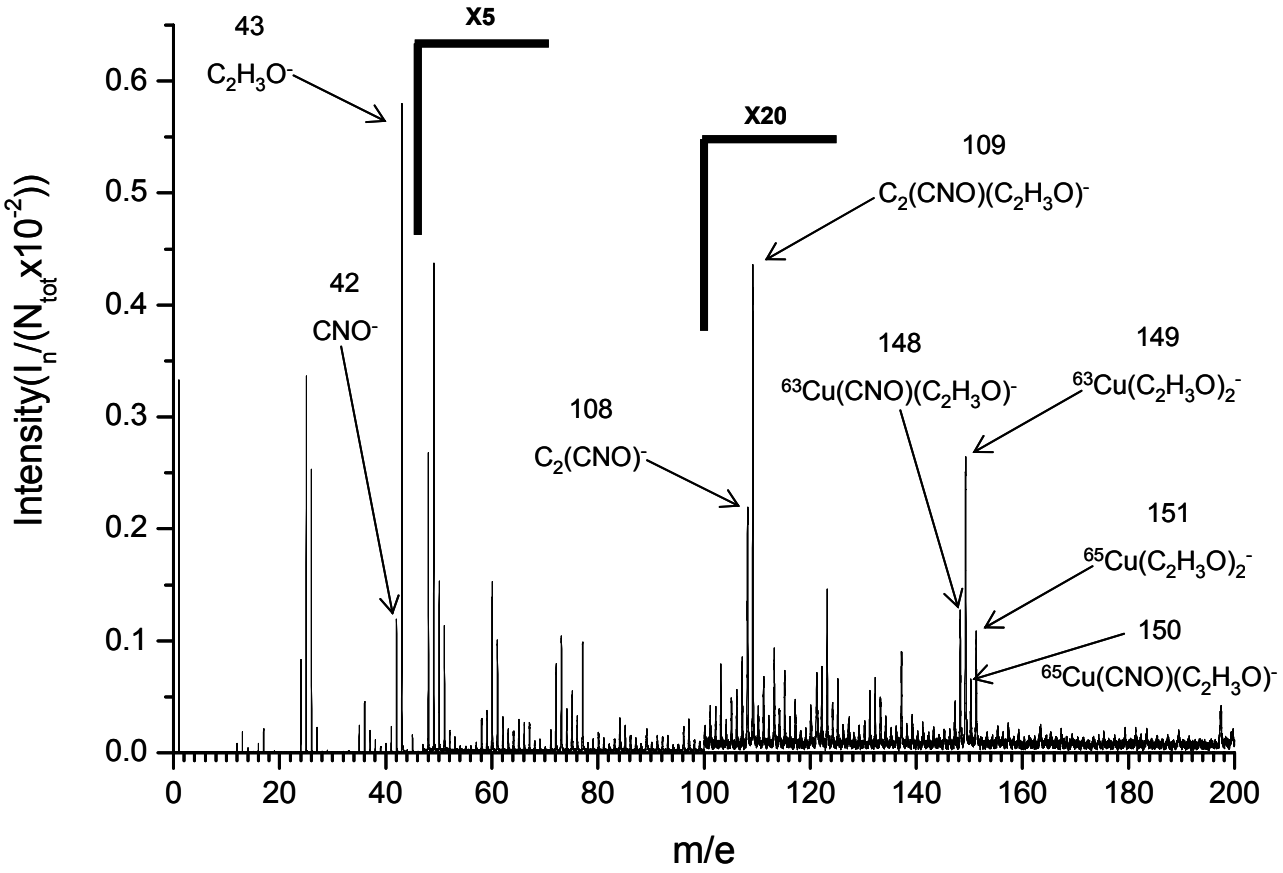

Figure 4-2. Cluster SIMS 116keV Au_{200}^{4+} spectrum of Cu aggregates on Si wafer.

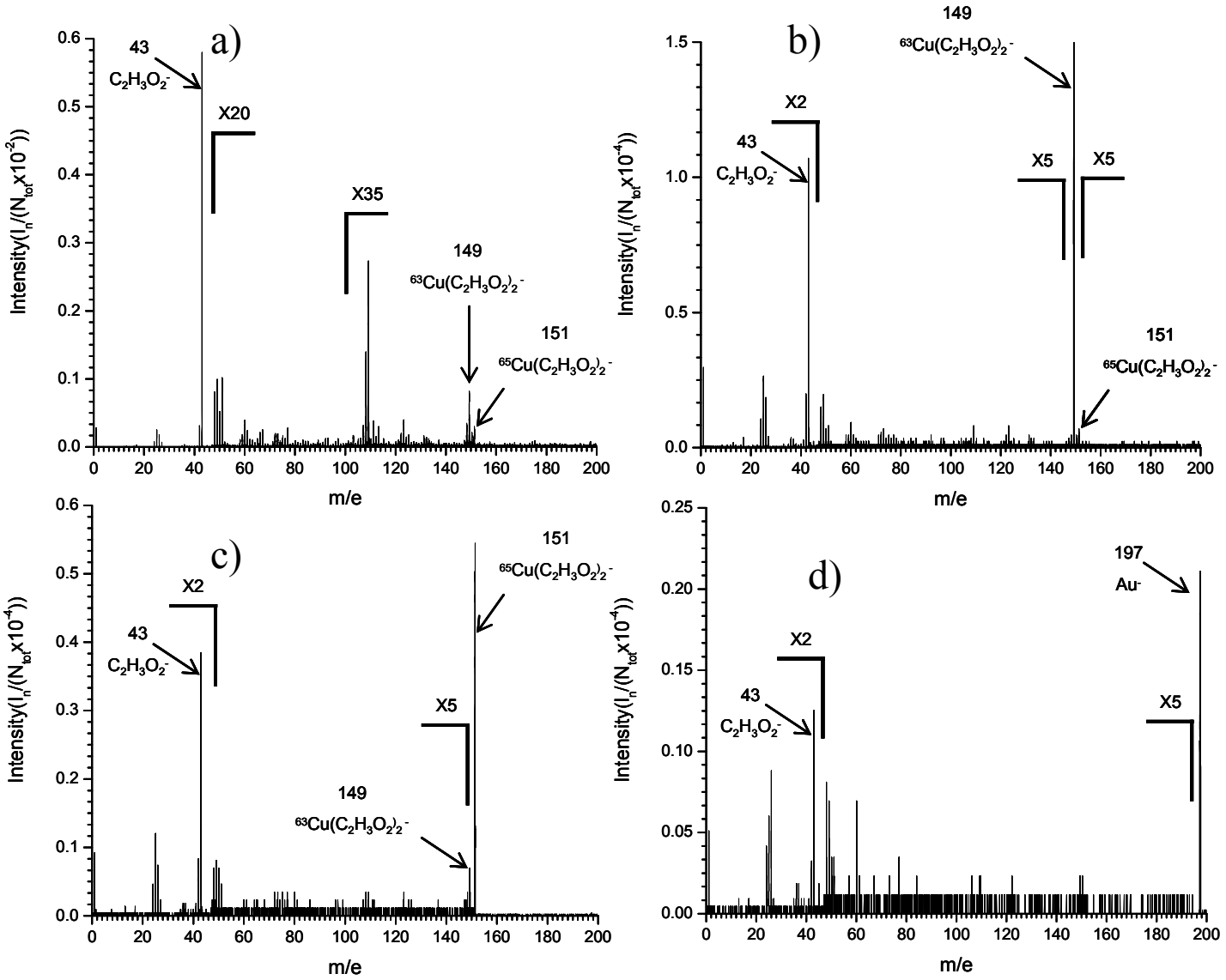

Figure 4-3. Mass spectra of ions co-emitted with a) m/e 43, b) m/e 149, c) m/e 151, and d) m/e 197 from a target consisting of Cu aggregates via cluster SIMS 116keV Au_{200}^{4+}.

Table 4-1. Peak areas of predominant secondary ion peaks in the mass spectrum of Cu aggregates on Si wafer produced by the bombardment of 116keV Au_{200}^{4+}.

		Cu Aggregates Peak Areas	
m/z	Fragment	Total Spectrum	Coincidence with m/z 43
1	H^-	63814	4918
43	$C_2H_3O^-$	233586	233023
148	$^{63}Cu(CNO)(C_2H_3O)^-$	4619	637
149	$^{63}Cu(C_2H_3O)_2^-$	10550	1458
150	$^{65}Cu(CNO)(C_2H_3O)^-$	2556	288
151	$^{65}Cu(C_2H_3O)_2^-$	4144	564

Table 4-2. Peak area ratios of predominant secondary ion peaks in the mass spectrum of Cu aggregates on Si wafer produced by the bombardment of 116keV Au_{200}^{4+}.

	Cu Aggregates Peak Area Ratios	
m/e Ratios	Total Spectrum	Coincidence with m/z 43
43/1	3.6604	47.3817
148/1	0.0724	0.1295
149/1	0.1653	0.2965
150/1	0.0401	0.0586
151/1	0.0649	0.1147
1/43	0.2732	0.0211
148/43	0.0198	0.0027
149/43	0.0452	0.0063
150/43	0.0109	0.0012
151/43	0.0177	0.0024
150/148	0.5534	0.4521
151/149	0.3928	0.3868

predominant peaks are $C_2H_3O^-$ and the coincidental ion peaks. The intensity of the $C_2(CNO)^-$ (m/e 108) and $C_2(CNO)(C_2H_3O)^-$ (m/e 109) peaks are greatly reduced in the coincidence spectra because these fragments were produced when the projectile bombarded the PVP coated Si wafer. Since the emission area is within the size of the Cu aggregates, copper-PVP fragments were sputtered from the surface when a projectile bombards a Cu aggregate.

In Fig. 4-4, the mass spectrum shows that the AuCu alloy sample produced peaks at m/e 394 and 592 which may be attributed to Au_2^- and Au_3^-, respectively. Peaks $^{63}CuAu_2^-$ (m/e 457) and $^{65}CuAu_2^-$ (m/e 459) are detected also in the mass spectrum (Fig. 4-4) of AuCu alloy sample. Due to the low intensity of m/e 457 and 459 peaks, it was impossible to obtain a coincidental mass spectrum for either of those peaks with good statistical data. However, the peak area ratio of m/e 459 to 457 was 0.396 which is close to the copper isotopic ratio 0.446. Because the current instrumental design is limited to the detection of negative secondary ions, it is not possible to detect the copper isotopes themselves using this method. Further experiments were undertaken to analyze the samples for copper, namely plasma desorption and laser ablation inductively coupled mass spectrometry.

PDMS

PDMS spectra were obtained for Cu aggregates, AuCu aggregates, AuCu alloy, Cu Foil and Si substate, i.e. blank (Figs. 4-5- 4-9). These spectra are dominated in the low-mass range by non-specific molecular fragments originating from contaminations.

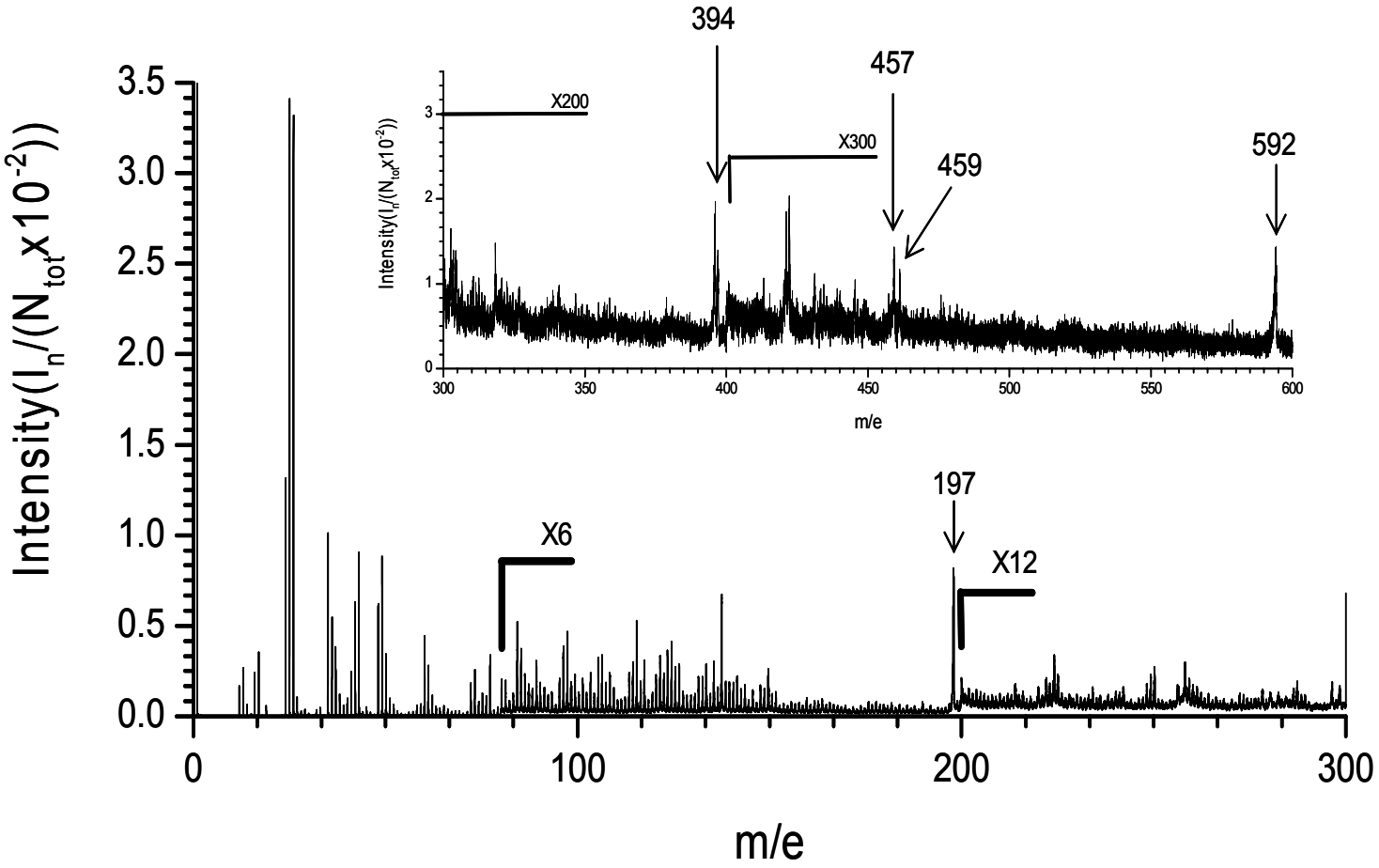

Figure 4-4. Cluster SIMS 116keV Au_{200}^{4+} spectrum of AuCu alloy on Si wafer.

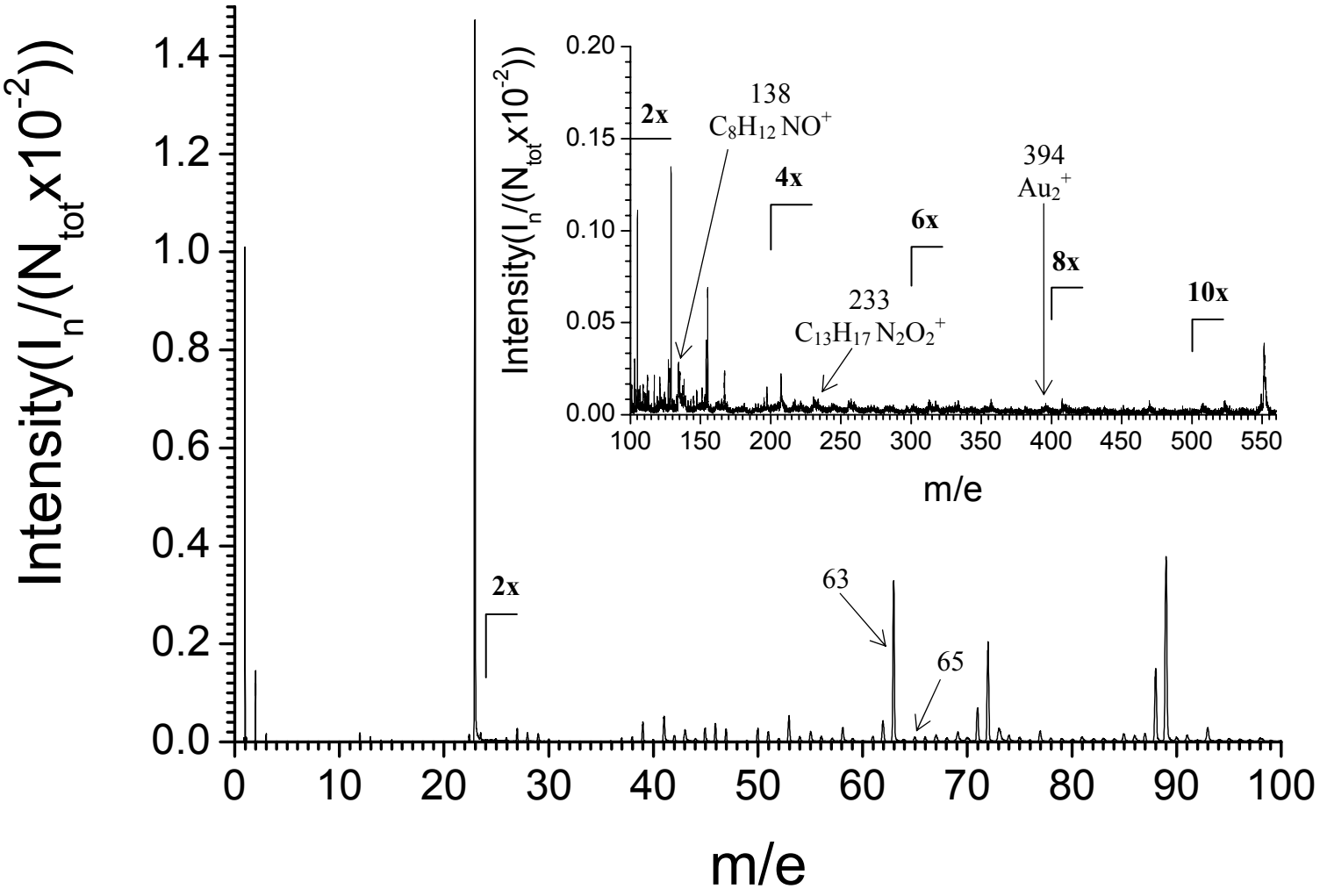

Figure 4-5. PDMS spectrum of Cu aggregates on Si wafer.

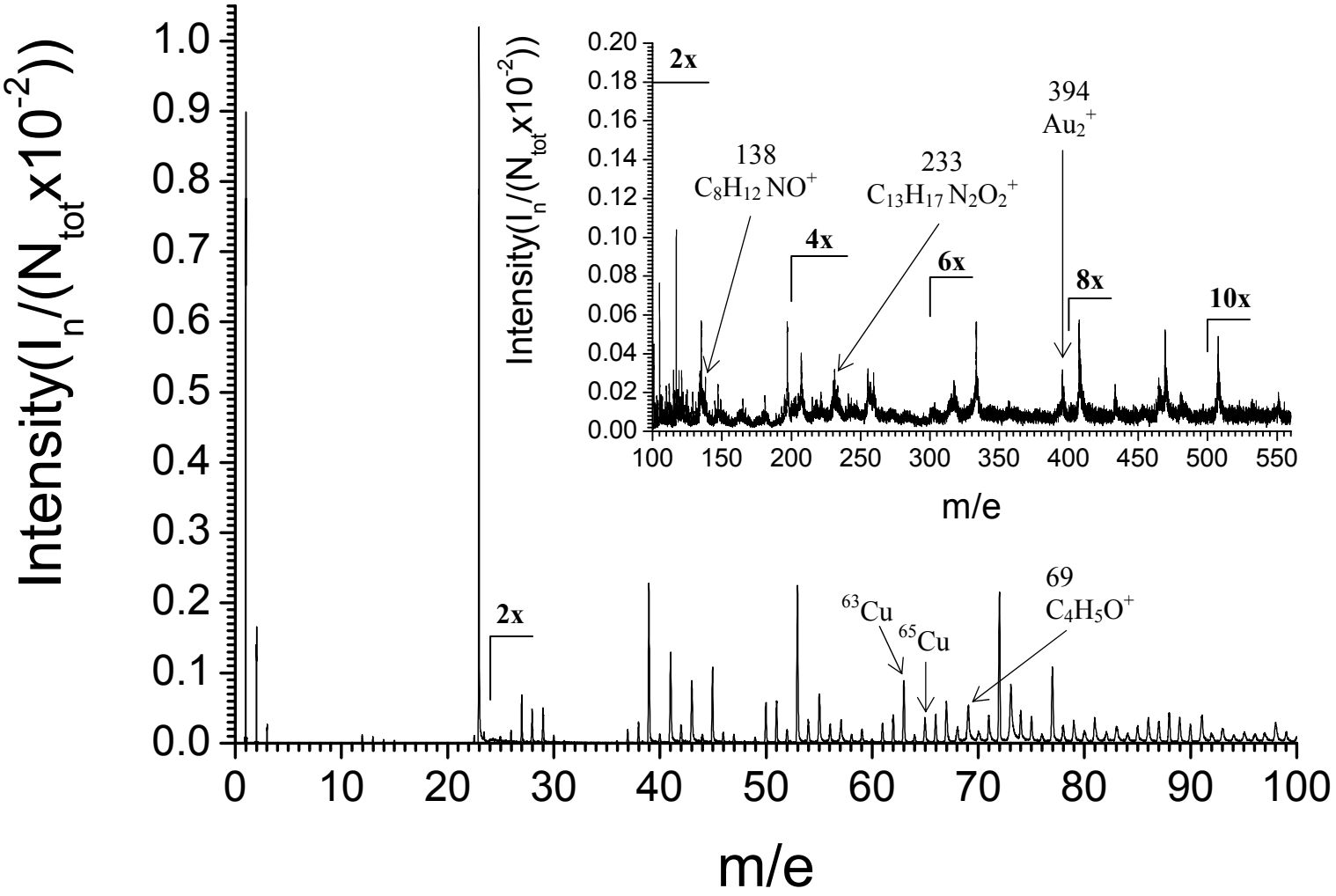

Figure 4-6. PDMS spectrum of AuCu aggregates on Si wafer.

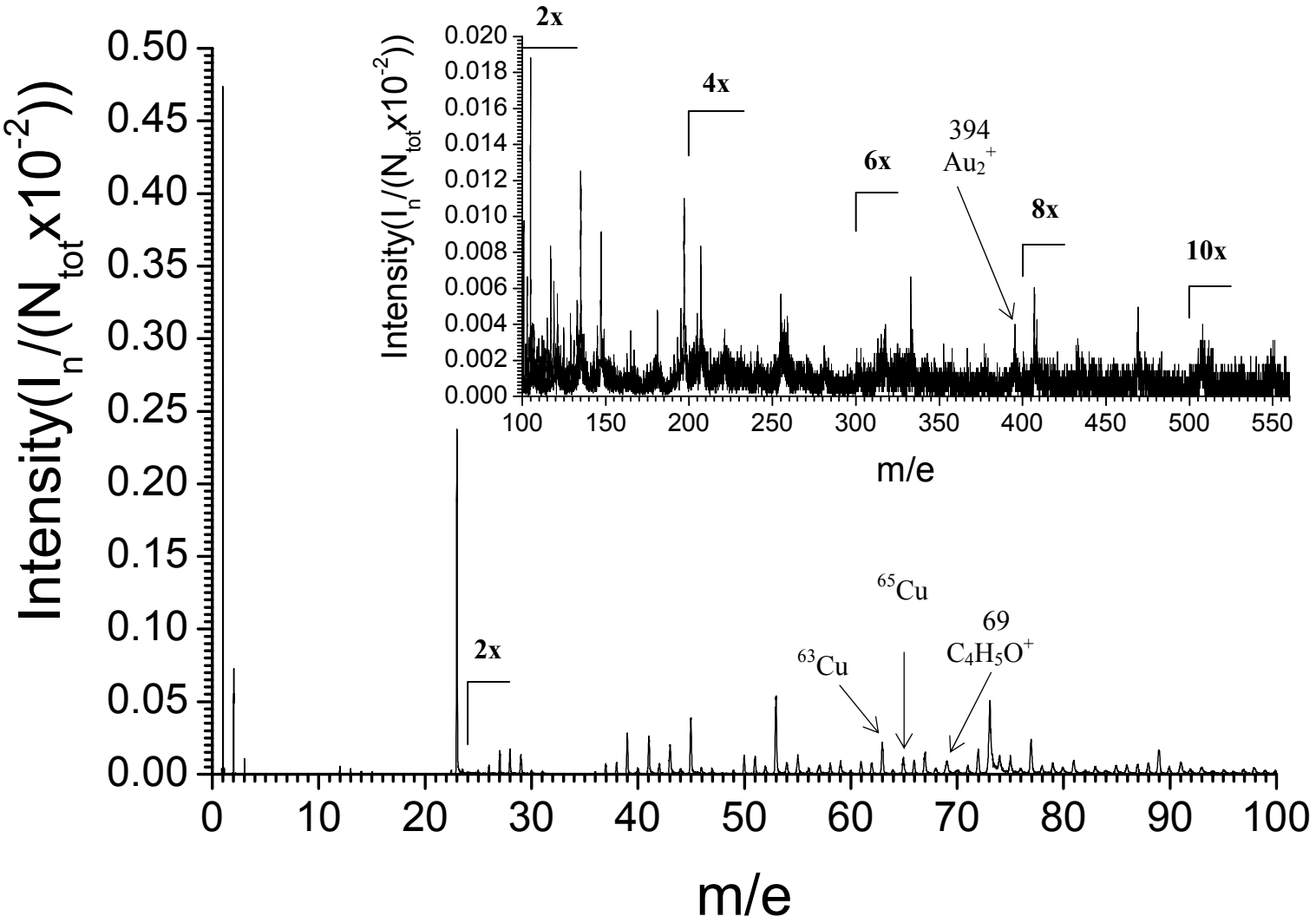

Figure 4-7. PDMS spectrum of AuCu alloy on Si wafer.

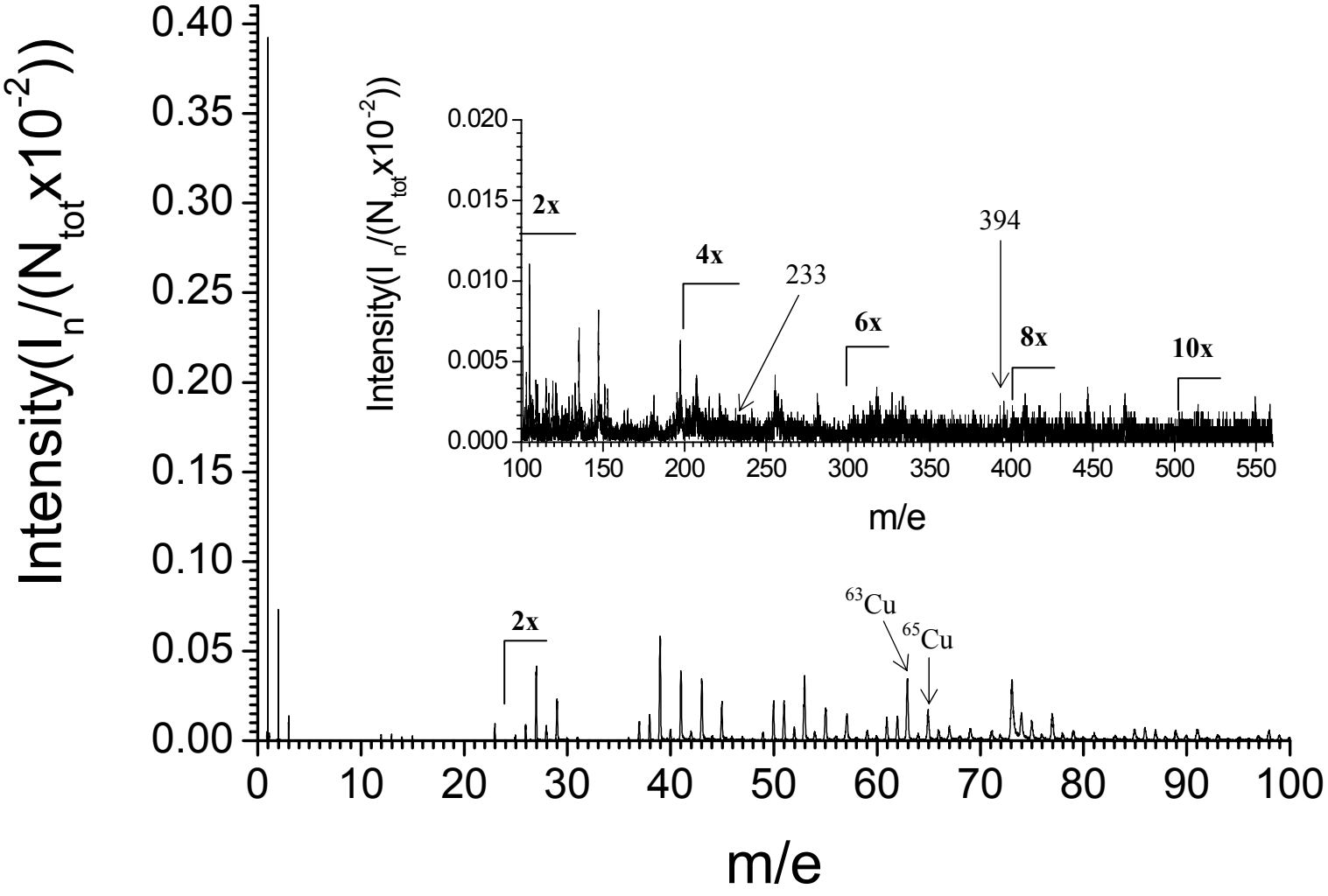

Figure 4-8. PDMS spectrum of Cu foil.

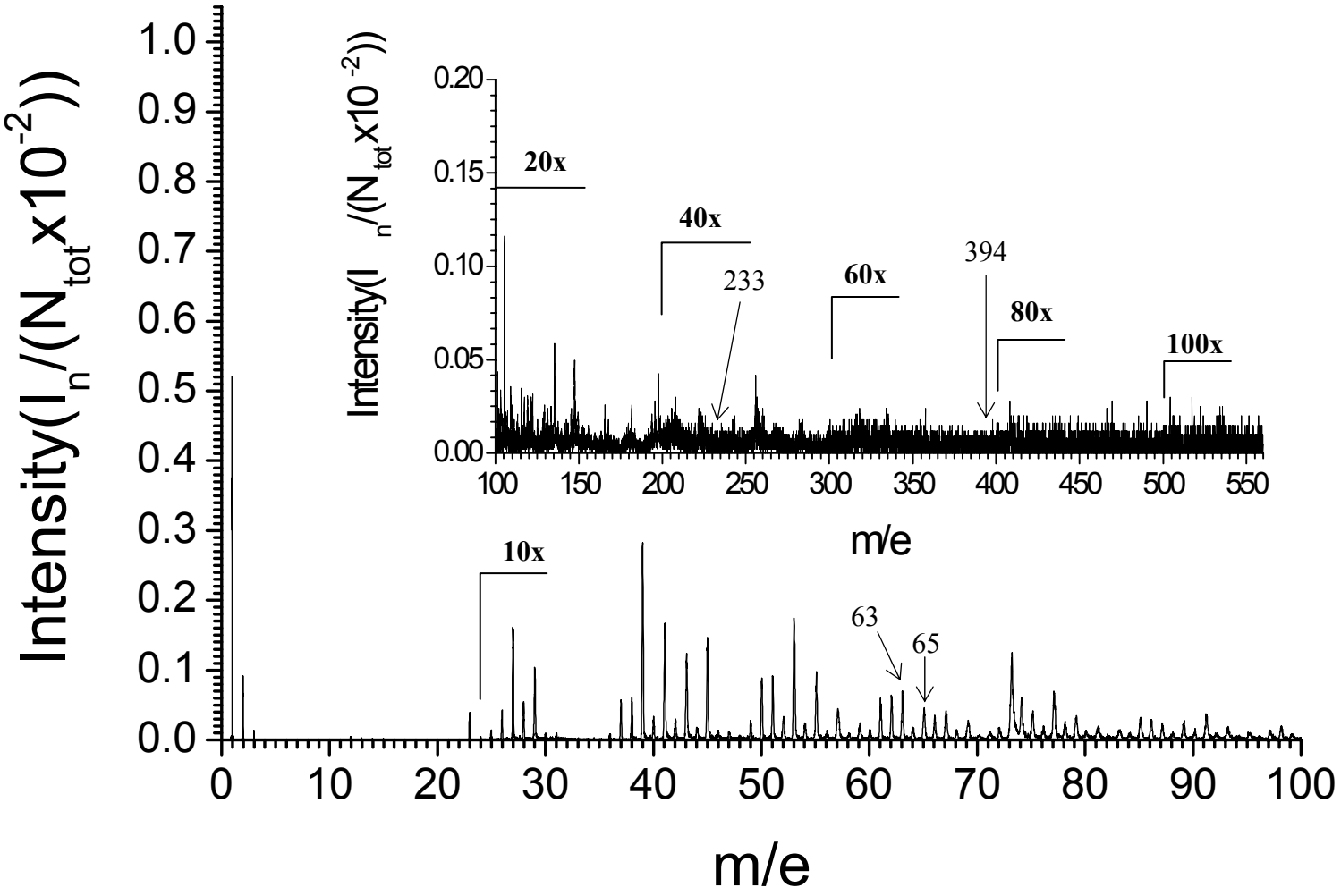

Figure 4-9. PDMS spectrum of Si wafer.

In the low and high mass region, the source of molecular signals in the mass spectra of the AuCu aggregates and Cu aggregates is the fragmentation of poly(vinylpyrrolidone) (PVP) stabilizer. Peaks with m/e 69 ($C_4H_5O^+$), 138 ($C_8H_{12}NO^+$), and 233 ($C_{13}H_{17}N_2O_2^+$) are due to the poly(vinylpyrrolidone) (PVP) stabilizer.

The peak areas for m/e 1, 12, 63 and 65 were obtained from the total spectrum of a Si wafer, Cu foil, and AuCu aggregates sample are listed in Table 4-3. In the spectrum of the Si wafer, the ratio of m/e 65 to 63 was 0.7754. That same ratio in the spectrum of AuCu aggregates decreased to 0.5143 which was close to the known copper isotopic ratio 0.446. A Cu foil was also analyzed via PDMS. The ratio of m/e 65 to 63 was 0.4933. The various observed ratios of m/e 63 and 65 increased in the AuCu samples. This is an indication that Cu is present in the sample but qualitative analysis is problematic because there is an interference with peaks at m/e 63 and 65 from contaminants.

A comparison between the spectra of Si substrate and AuCu aggregates suggested that m/e 394 may indicate the presence of Au_2^+. However, a comparison of the AuCu precursor and ozone cleaned precursor spectra revealed that the peak at m/e 394 is due to the polymer. The concentration of Au in the sample is not sufficient to recognize peaks associated with gold. It is thought that the if there was enough of the AuCu precursor aggregates on the Si wafer, then PDMS was unable to produce fragments from the aggregates because this technique only samples the top most layer. In these samples, the top most layer was PVP. This is further supported by the mass spectrum of Cu aggregates (Fig. 4-4). There is a predominant peak at m/e 63 and a peak

of low intensity at m/e 65. The peak area ratios of these peaks to do not correspond to the isotopic ratio of copper therefore it is unclear if the sample contains copper. To verify that the sample contained copper, further experiments were done with LA-ICP-MS.

LA-ICP-MS

Laser ablation inductively coupled plasma mass spectrometry (LA-ICP-MS) was used to verify the presence of Au and Cu in all of the nano-particle samples used in this experiment. The analysis of AuCu precursor, AuCu intermetallic, AuCu alloy and Cu aggregates yielded the spectrum in Fig. 4-11. Once that sample was introduced into the LA-ICP-MS sample chamber, an acquisition took about one and half minutes, whereas, each of the SIMS acquisitions required about one hour and the PDMS acquisitions were approximately 120 hours in duration.

The LA-ICP-MS instrument can only provide isotopic information about the AuCu and Cu aggregates samples. It is shown in Fig. 4-10 that the AuCu samples contained both ^{197}Au and ^{63}Cu while the Cu aggregate sample contained only ^{63}Cu. LA-ICP-MS is a sample destructive technique. In Fig. 4-11, the raster pattern, with spacing of 100 μm and a depth of emission of 5 μm, can be seen in the image of the sample surface which was ablated.

Table 4-3. Peak area ratios of m/e 1, 12, 63, and 65 peaks in the mass spectrum of Si wafer, AuCu aggregates on Si wafer, and Cu foil via positive Plasma Desorption Mass Spectrometry.

Postive Plasma Desorption Mass Spectrometry Peak Areas										
	m/e				m/e Ratios					
	1	12	63	65	65/63	63/1	65/1	12/1	63/12	65/12
Fragment	H^+	C^+	$^{63}Cu^+$	$^{65}Cu^+$	$^{65}Cu^+/^{63}Cu^+$	$^{63}Cu^+/H^+$	$^{65}Cu^+/H^+$	C^+/H^+	$^{63}Cu^+/C^+$	$^{65}Cu^+/C^+$
Si Wafer	81621	956	1692	1312	0.7754	0.0207	0.0161	0.0117	1.7699	1.3724
AuCu Aggregates	152801	2380	10063	5175	0.5143	0.0659	0.0339	0.0156	4.2282	2.1744
Cu Foil	65775	699	5157	2544	0.4933	0.0784	0.0387	0.0106	7.3777	3.6395

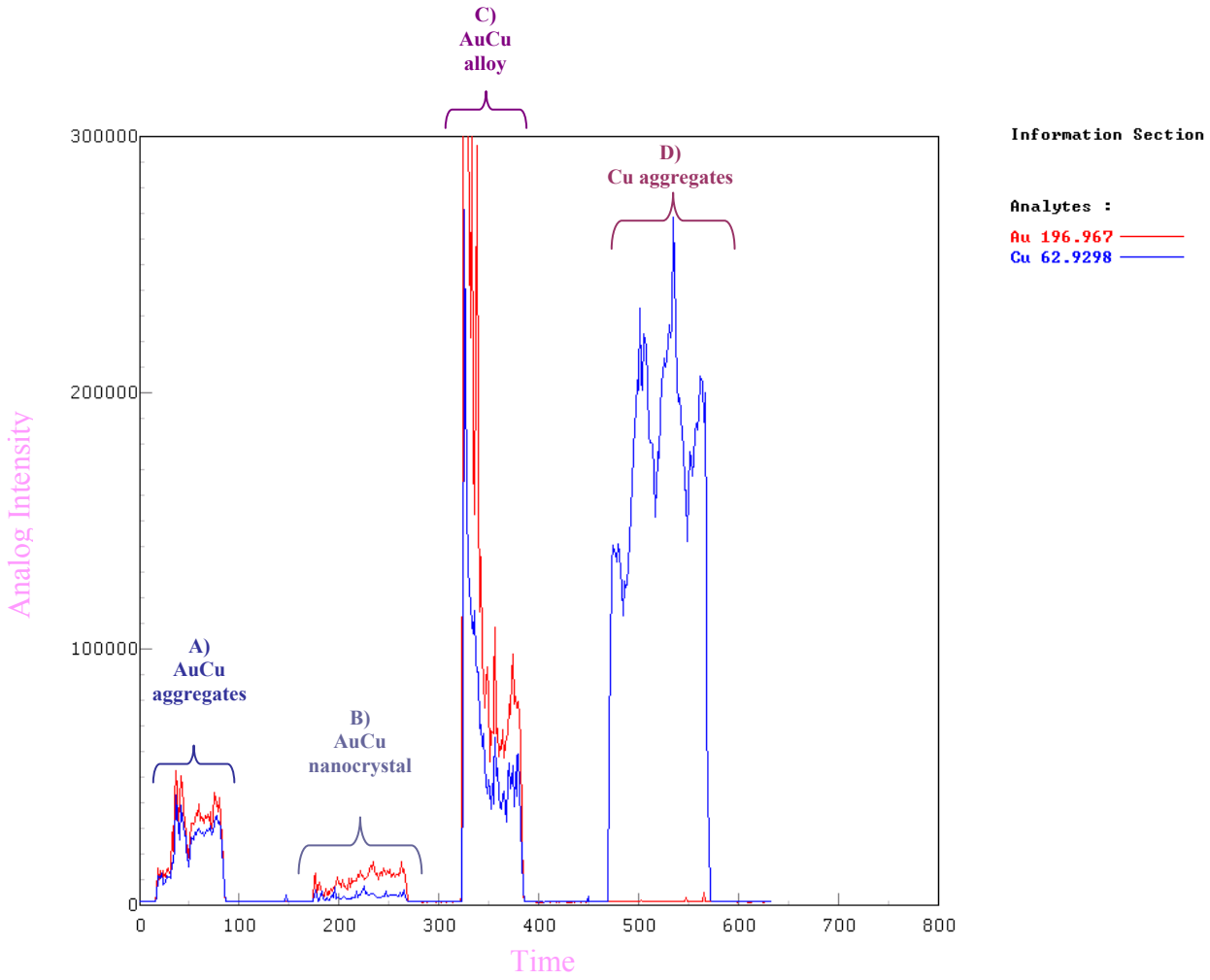

Figure 4-10. LA-ICP-MS spectra of a) AuCu aggregates, b) AuCu nanocrystal, c) AuCu alloy, and d) Cu aggregates.

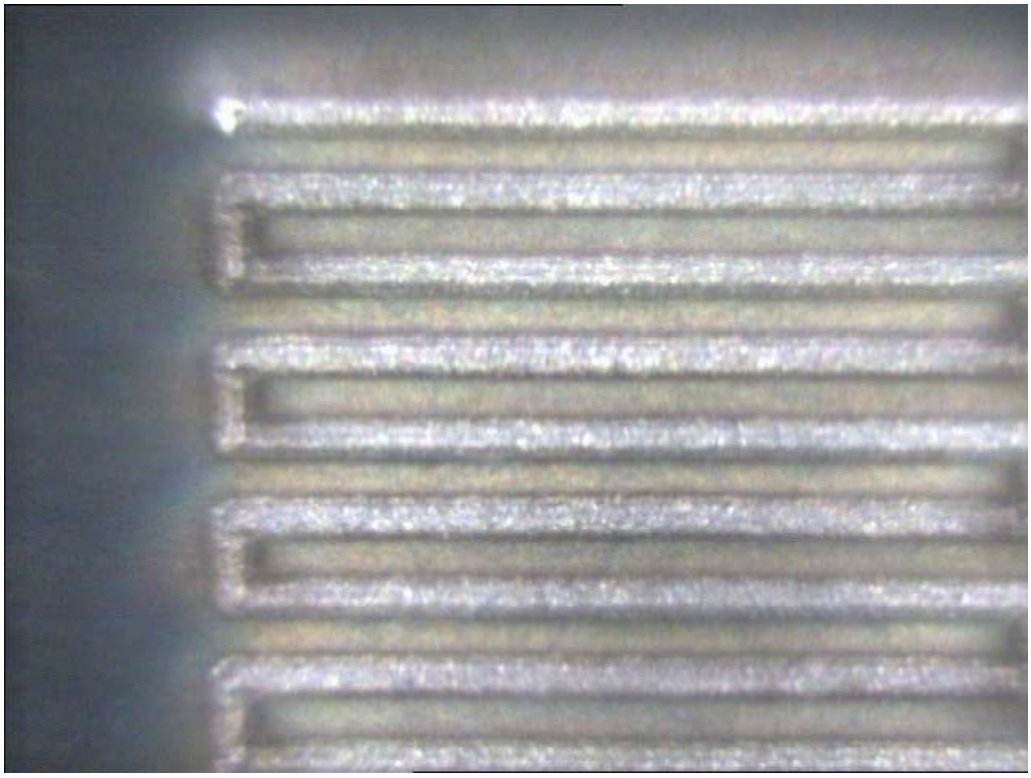

Figure 4-11. Image of AuCu alloy sample after undergoing analysis by LA-ICP-MS.

CHAPTER V

COINCIDENCE ION MASS SPECTROMETRY OF α-ZrP

The number of secondary ions detected from a single MeV projectile impact varies depending on the target. Events in which multiple secondary ions are detected are interesting from both a fundamental and applied prospective. From the applied perspective, events in which two or more secondary ions are ejected can provide chemical information from an area just a few nanometers in diameter. This technique has been used for the investigation of nano-objects and interrogation of chemical micro-homogeneity on the nano-meter scale.

Previous investigations have revealed that the PDMS signal is sensitive to analyte surface structure. Specifically, the compound α-ZrP was investigated as an amorphous gel and again as a polycrystalline material over several microns. Although the stoichiometry remains the same in both samples, the mass spectra show qualitative differences, which can be attributed to physical structure. It was shown that negatively charged polyatomic secondary ions are ejected by the direct emission processes and are fragments representative of the surface structure [25].

The aim of this research was to investigate how surface structure influences events in which multiple secondary ions are detected. The TME data acquisition software is used in conjunction with both cluster SIMS and PDMS as an efficient approach to record all events, i.e. all secondary ions detected from each primary projectile impact. We measured the yield of specific α–ZrP fragments emitted as a

function of the total number of secondary ions emitted in single impact events. Targets were prepared by mixing 0.05g of the ZrP into 1 mL ethanol, and depositing 50 μL of the slurry onto a stainless steel target.

Based on the previous experiments, the peak areas for several fragment ions that were traced back to the crystal structure of α-ZrP were collected via the TME software. These fragments with the m/e: 79, 282, and 343 (Fig. 5-1) were chosen because preliminary results indicate that ion yields were adequately abundant in various single impact events for both the gel and crystalline α–ZrP targets [25].

SIMS

Figure 5-2 is a cluster SIMS mass spectrum of α-ZrP gel. The most prominent peaks in this mass spectrum are those with m/e 63, PO_2^- and 79, PO_3^-. Most of the higher, structure-specific mass fragments are in low abundance. This has been attributed to the lack of long range ordering, on the scale of the emission area [26]. Figure 5-3(a) is a powder diffraction spectrum of the same sample. The peaks are broad suggesting some evidence of structure in the gel. This may explain why some structure-specific fragments are present in the mass spectrum of the gel sample, Fig. 5-2. Figure 5-4 is a mass spectrum of a crystalline α-ZrP sample. Again, the two predominant peaks are m/e 63 and 79. However, the structure-specific fragments are much more abundant. The presence of these peaks can be attributed to the fact that the surface is ordered to a greater degree compared to the gel α-ZrP sample. A powder XRD spectrum, Fig. 5-3b, further supports this observation.

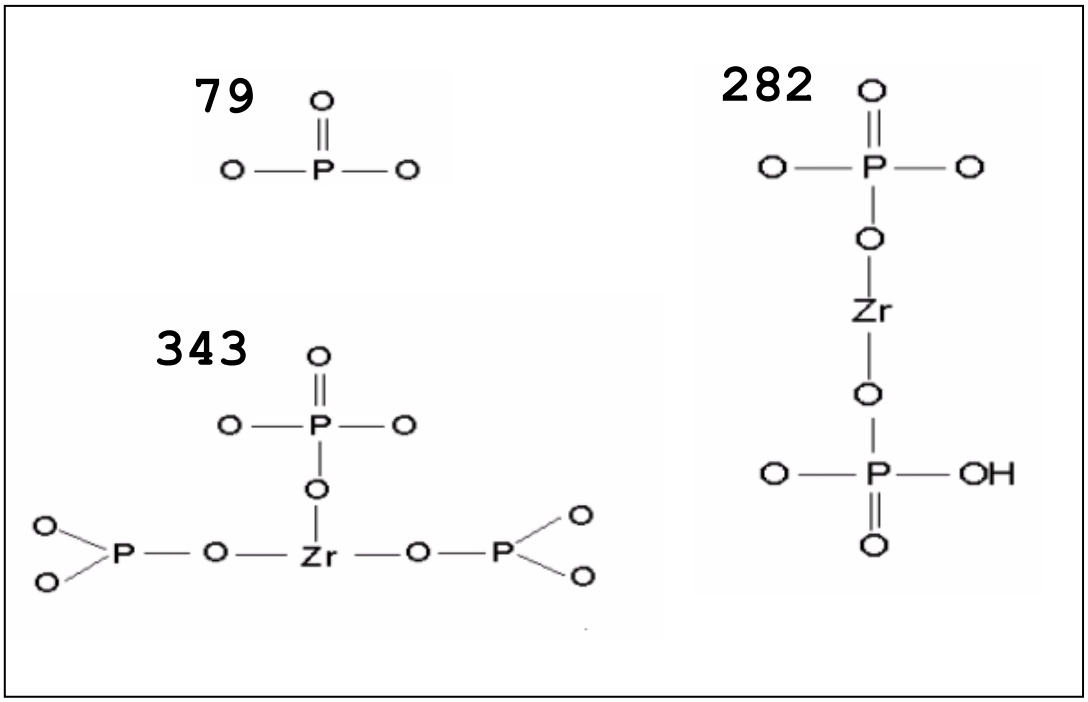

Figure 5-1. Structure specific fragment ions traced back to the crystal structure of α-ZrP.

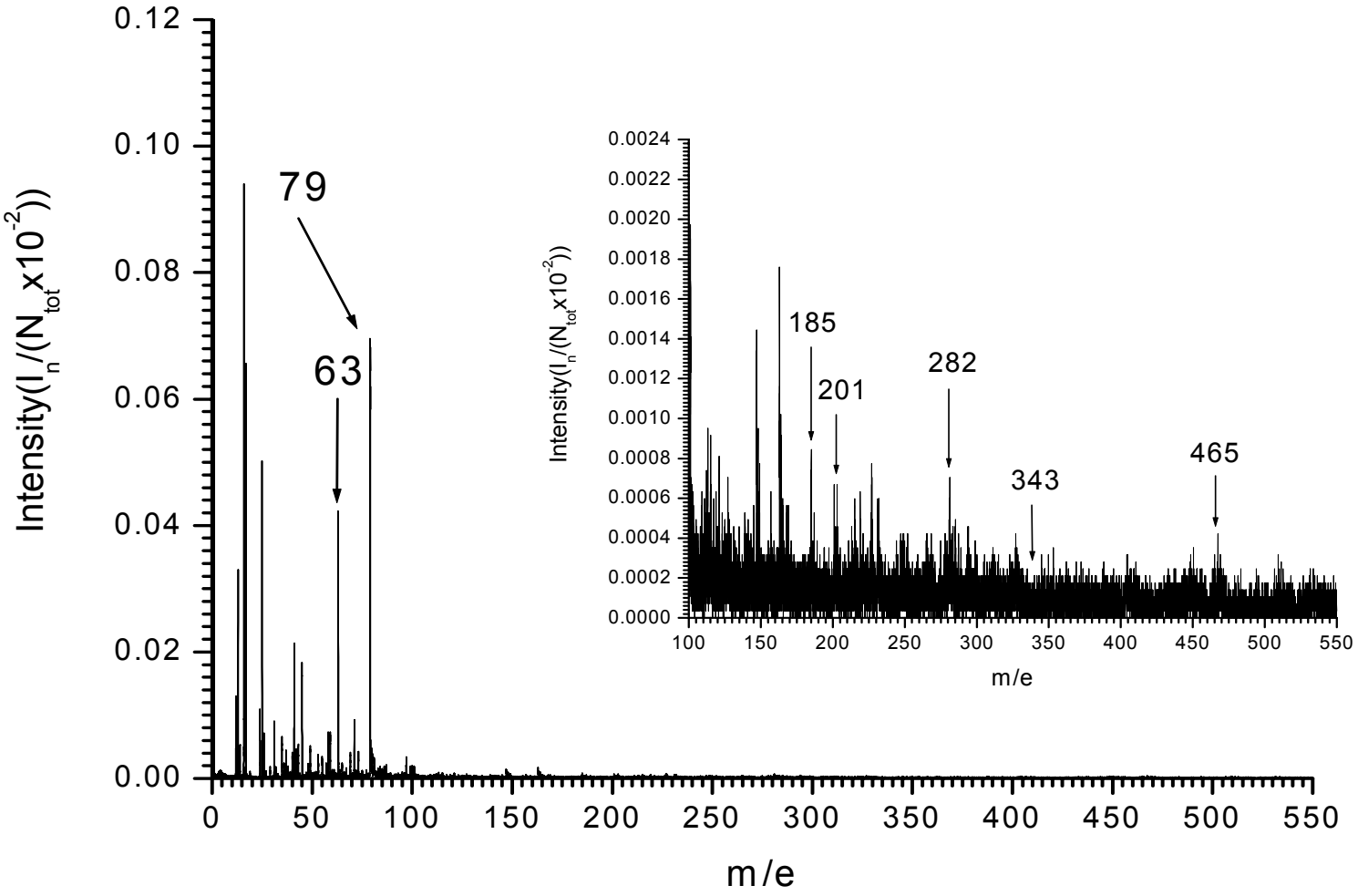

Figure 5-2. Cluster SIMS mass spectrum of α-ZrP gel.

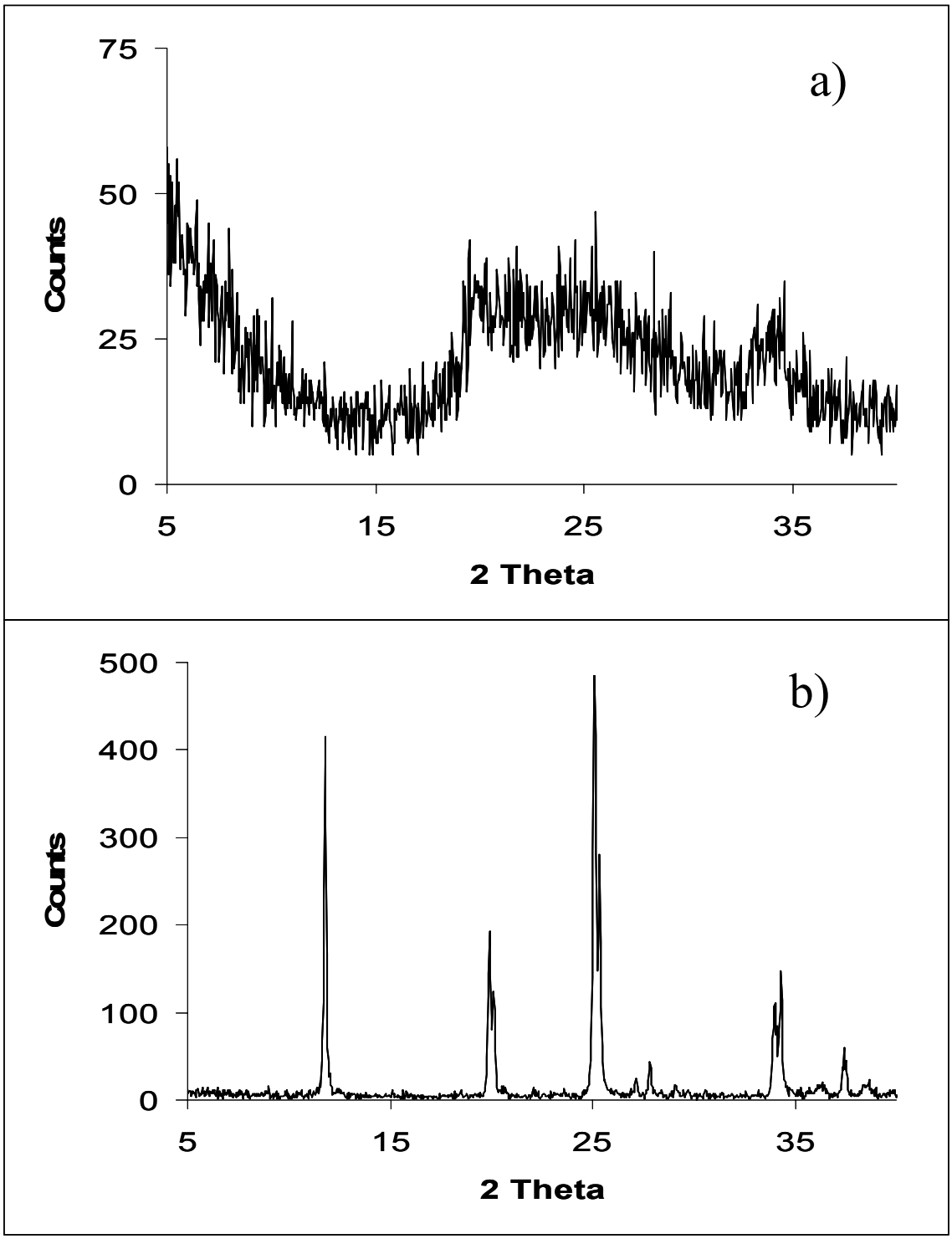

Figure 5-3. Powder XRD spectrum of a) α-ZrP gel and b) crystalline α-ZrP material.

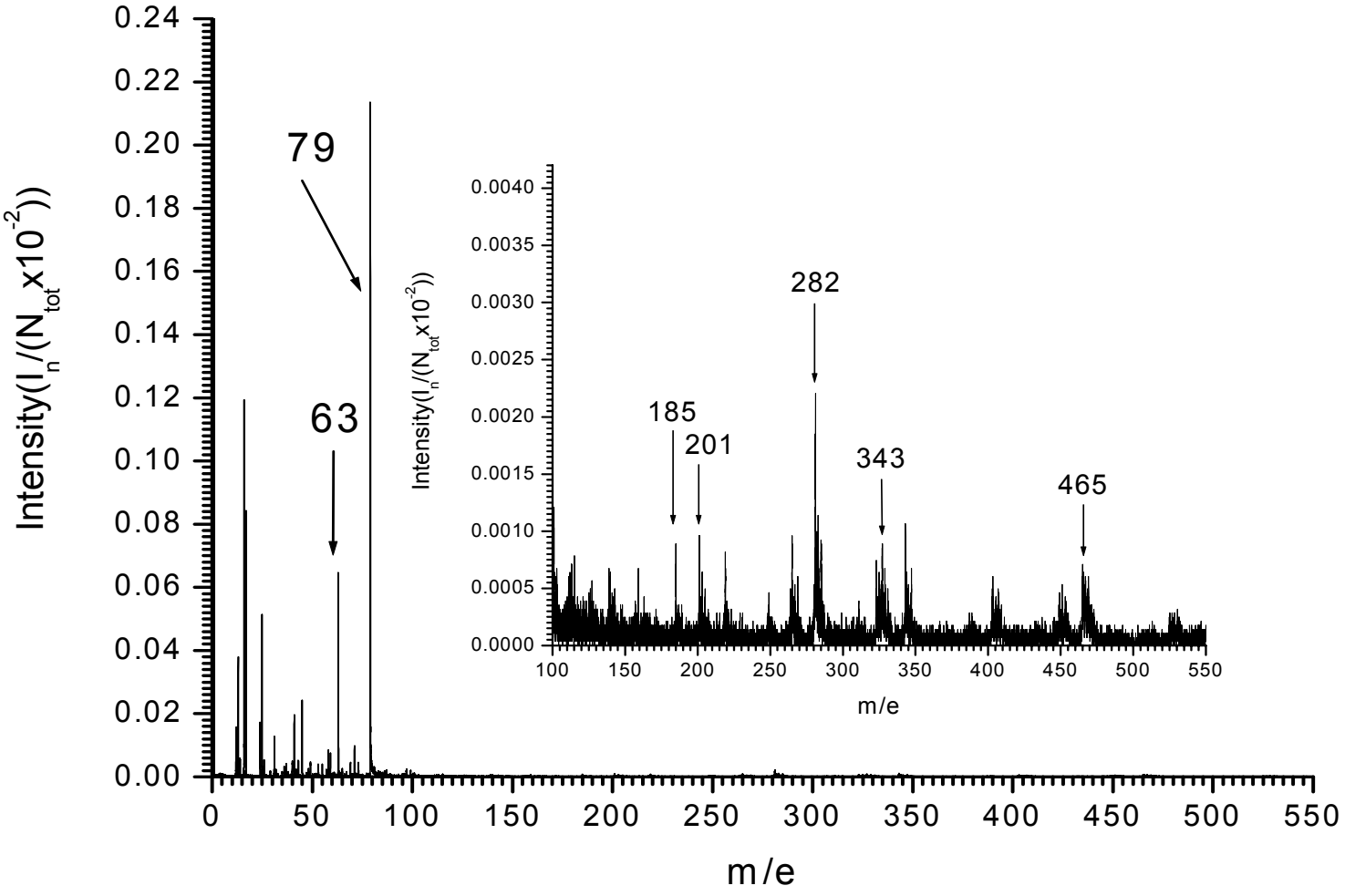

Figure 5-4. Cluster SIMS mass spectrum of crystalline α-ZrP.

The aim of this research was to investigate how surface structure influences events in which multiple secondary ions were detected. The TME software allowed the yield of specific α–ZrP fragments emitted as a function of the total number of secondary ions emitted in single impact events to be measured. In this investigation, the yield of m/e 79, 282 and 343 were plotted as a function of the total number of secondary ions ejected per single impact event for the gel and crystalline samples. Figure 5-5(a) reveals that as the yield of PO_3^- decreases for the crystalline sample, the PO_3^- remains relatively constant for the gel sample. The yields for fragments with m/e 282 and 343 plotted in Figures 5-5(b) and 5-5(c), respectively, revealed an opposite trend. The yield of these mass fragments in the crystalline sample increases as the number of secondary ions ejected per event increase.

PDMS

PDMS results were comparable to the results obtained from the cluster SIMS results. Most of the higher, structure-specific mass fragments are in low abundance for the gel ZrP sample, Fig. 5-6. For the crystalline ZrP sample, the structure-specific fragments are much more abundant in Fig. 5-7. The yield of m/e 79, 282 and 343 plotted in Fig. 5-8 revealed similar trends seen in the results from the cluster SIMS experiments. Figure 5-8(a) indicated that the yield of m/e 79 remained fairly constant for the gel ZrP sample while the yield corresponding to the same fragment in the crystalline sample increased with the number of secondary ions ejected per event.

Figures 5-8(b) and 5-8(c) show that the yields for m/e 282 and 343 in the crystalline sample increases as the number of secondary ions ejected per event increase.

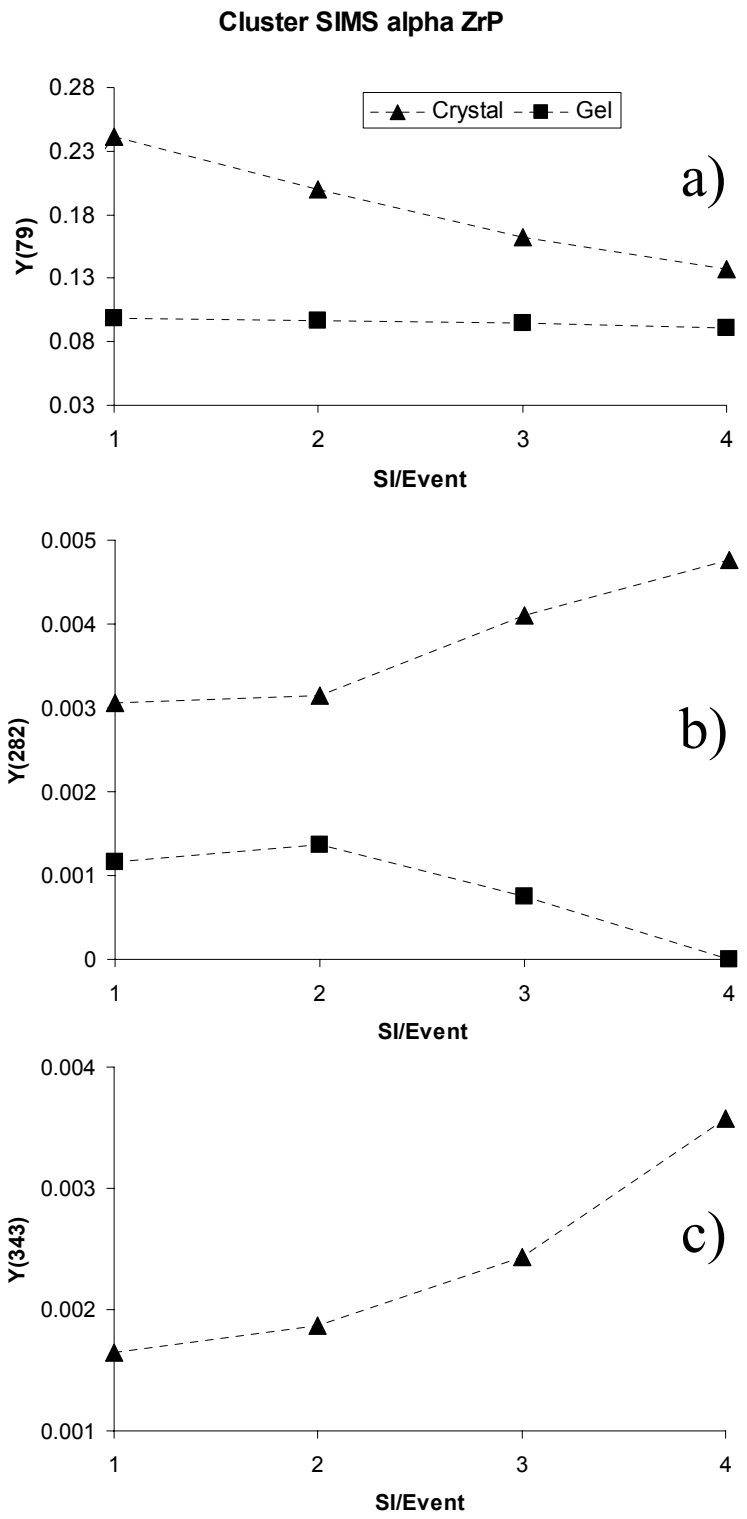

Figure 5-5. Yield of a) m/e 79, b) m/e 282, and c) m/e 343 as a function of the total secondary ions ejected per single impact event via cluster SIMS.

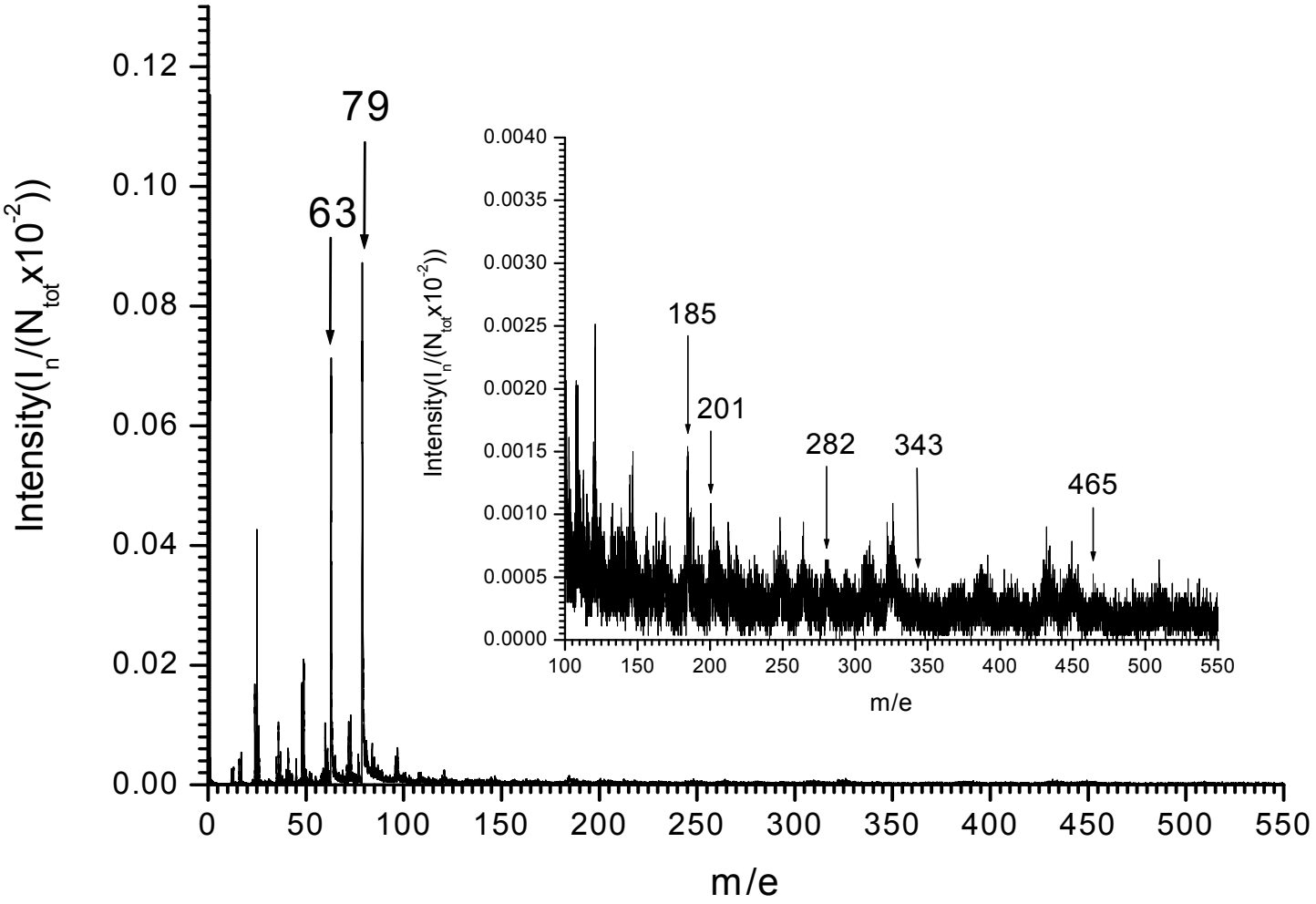

Figure 5-6. PDMS mass spectrum of gel α-ZrP.

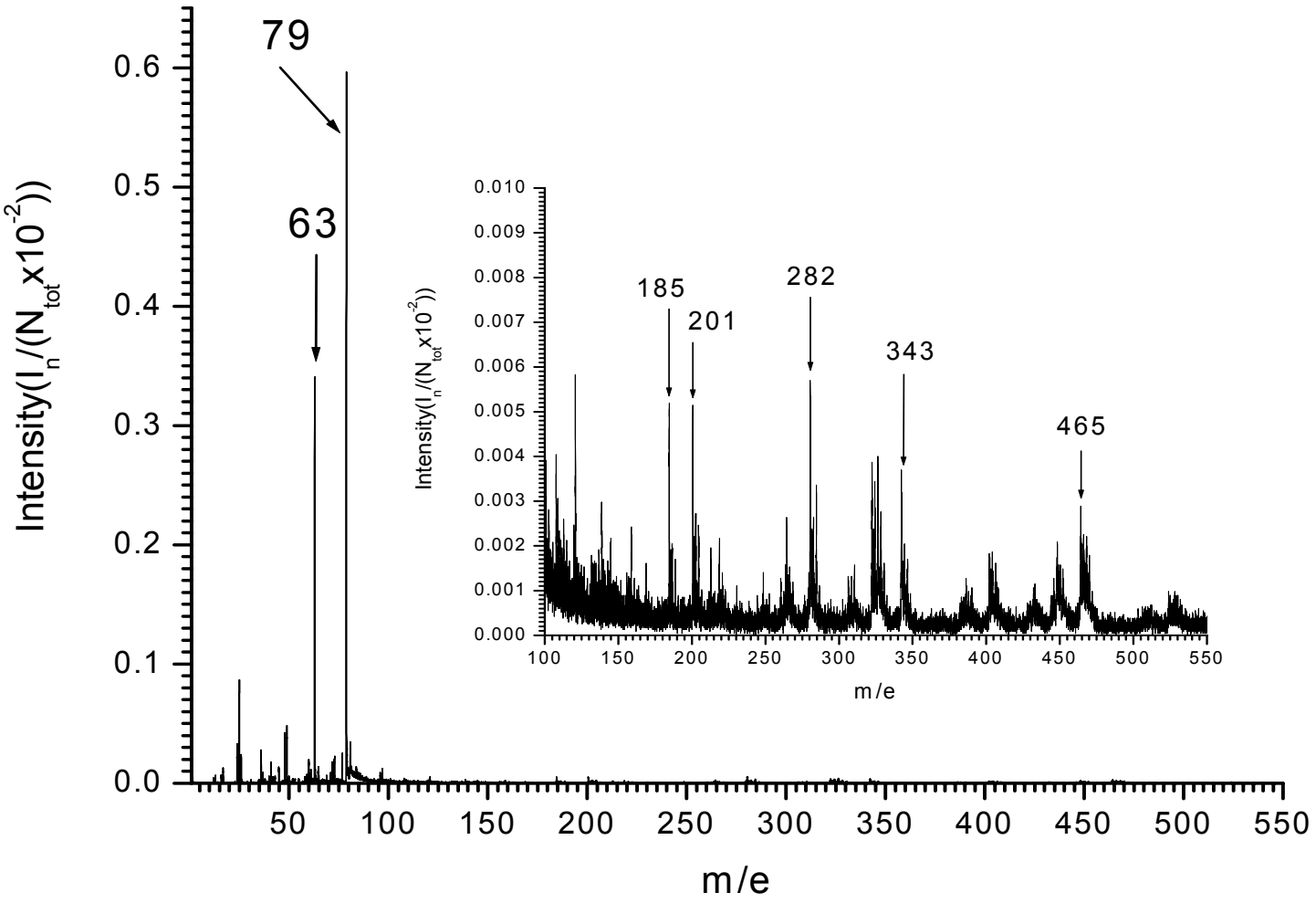

Figure 5-7. PDMS mass spectrum of crystalline α-ZrP.

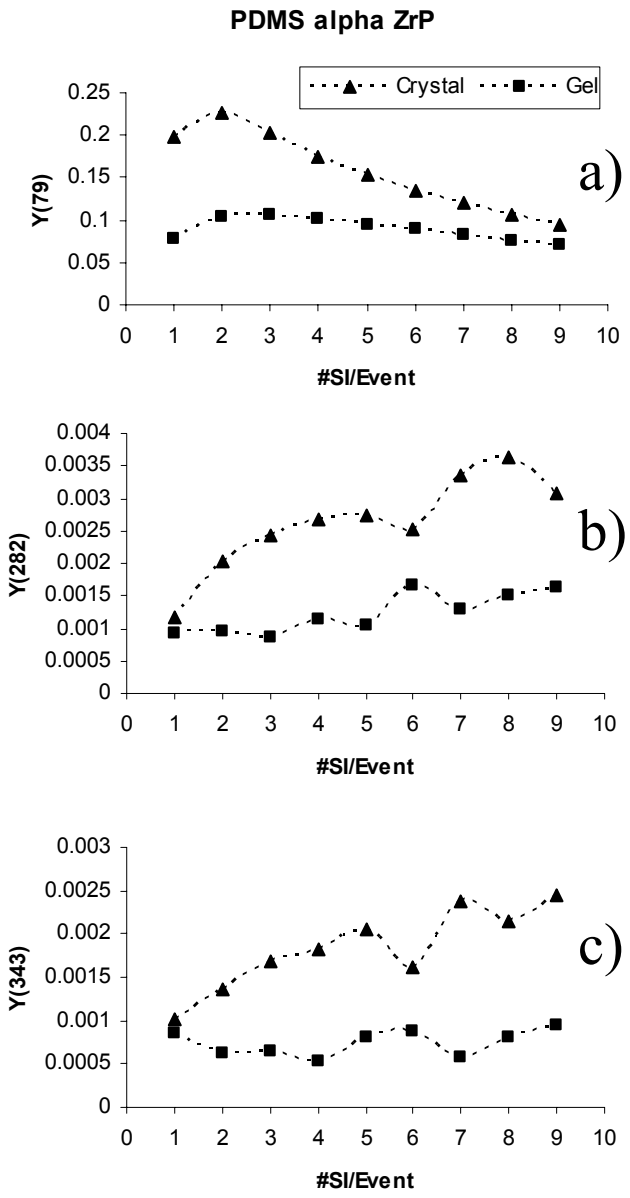

Figure 5-8. Yield of a) m/e 79, b) m/e 282, and c) m/e 343 as a function of the total secondary ions ejected per single impact event via PDMS.

CHAPTER VI

CONCLUSIONS

One of the objectives of this research was to validate chemical analysis in the nano-domain regime via coincidence ion emission spectrometry. For this investigation, photooxidized Au nanorods with at MHDA monolayer were bombarded with 17keV Au_3^+ projectiles to produce secondary ion emissions. Data processed by utilizing the TME software yielded a mass spectrum of molecular fragments co-emitted with m/e 197 (Au^-). Results indicate that SO_3^- fragment was co-emitted with Au^-. This verifies that the thiol monolayer exists on the Au nanorods surface. The coincidence spectrum for Au sputtered off of a bare Au nanorod revealed a decrease in the intensity for the SO_3^- fragment peak. Therefore, it is not conclusive that the monolayer is directly attached to the Au nanorod surface. For this reason, the samples were also analyzed via PDMS.

A positive PDMS spectrum of Au nanorods soaked in 16-mercaptohexadecanoic acid revealed a molecular fragment at m/e 507 which corresponds to the Au adduct molecule, $HAuS(CH_2)_{15}COONa^+$. From the literature, it is known that this adduct occurs because carboxylic acids generate a high-energy surface which contaminates rapidly in the laboratory atmosphere. The identification of this peak is also supported by the abundant presences of a Na^+ peak. The intensity of Na^+ significantly decreases in the mass spectrum of Au 'bare' nanorods, and m/e 507 is absent. For further verification, a Au coated Si wafer which was soaked in MHDA was also analyzed via PDMS. Similar results were obtained for that sample. The mass spectrum of the Au coated wafer

covered with the MHDA monolayer also contained a peak at m/e 507 and the intensity of Na^+ was more abundant than in the spectrum for the bare Au coated Si wafer. A comparison of intensity ratios of OH^- and SH^- identified in the negative plasma desorption mass spectra for each of the samples discussed previously indicated that the $HCO_2(CH_2)_{15}S^-$ monolayer is bonded to the Au nanorods. Further research must be done to verify if either of the previously discussed techniques can investigate orthogonal self-assembled monolayers on Au/Pt nanorods.

A series of samples consisting of copper and gold were also investigated by SIMS and PDMS to determine if either of these techniques are appropriate for characterizing these types of nanoparticles. The SIMS experiments of Cu aggregates showed that Au_{200}^{4+} is an effective projectile to investigate surface of the target because it was able to penetrate through the PVP stabilizer that coated the surface of the Cu aggregates. The bombardment of this target with the Au_{200}^+ projectile produced copper and PVP containing fragments such as CNO^- (m/e 42), $C_2H_3O^-$ (m/e 43), $C_2(CNO)_2^-$ (m/e 108), $C_2(CNO)(C_2H_3O)^-$ (m/e 109), $^{63}Cu(CNO)(C_2H_3O)^-$ (m/e 148), $^{63}Cu(C_2H_3O)_2^-$ (m/e 149), $^{65}Cu(CNO)(C_2H_3O)^-$ (m/e 150), and $^{65}Cu(C_2H_3O)_2^-$ (m/e 151). Coincidence spectra of $^{63}Cu(CNO)(C_2H_3O)^-$ (m/e 148) and $^{65}Cu(CNO)(C_2H_3O)^-$ (m/e 150) indicated that, when an aggregate is bombarded by a Au_{200}^{4+} projectile, emission is produced from the surface of the aggregate. A AuCu alloy sample was also investigated. This experiment produced peaks $^{63}CuAu_2^-$ (m/e 457) and $^{65}CuAu_2^-$ (m/e 459). However, the low number of events where $^{63}CuAu_2^-$ and $^{65}CuAu_2^-$ were emitted prevented data analysis by coincidental ion emission. Further analysis was preformed on these set of

samples via PDMS to detect positive secondary ions to determine the presence of Cu by the isotopic ratio of copper. The limitation of this technique was that it could not sample the surface of the aggregates because PDMS samples the top most layer of the target which was the PVP stabilizer. LA-ICP-MS was a technique that was utilized to determine the presence of copper and gold in the samples. However, this technique is only capable of identifying the isotopes in the samples but revealed no information about the chemical make up on the nano-surfaces.

Another objective of this project was to research the relationship between the type and abundance of SIs, and structure of ionic and molecular species in stoichiometric specific surface structures. Qualitative observations have revealed that samples with the same stochiometry but different surface structure influence the overall appearance of the mass spectra. More molecular fragmentation is observed in the mass spectrum corresponding to the more ordered surface structure, crystalline α-ZrP, than there is in the spectrum of gel α-ZrP. By examining the selected SI emission events, the results from the experiments performed on α-ZrP samples have shown that relative yields of certain fragments are dependent upon the surface ordering of the target. Further research in this area may look at samples were there are gradual changes in surface structure. It would be interesting to see if similar trends can be observed if the surface structures of the analytes vary slightly.

We have demonstrated, from a qualitative standpoint, that cluster SIMS can reveal changes in surface structure in the absence of any change in the analyte stoichiometry. Specifically, we show how the structure of the analyte can influence the

appearance of the overall mass spectra. Further information is available when monitor selected emission events, e.g. events when three or four secondary ion are ejected. We show how the relative yields of particular fragments, in multi-ion emission events, depend on the surface ordering of the target. Using this approach it may be possible to determine the relative degree of surface ordering in the target analyte. Future studies in the area of cluster CIMS should concentrate on exploring if the trends for secondary ion yields as a function of projectile characteristics observed here exist for other analyte-specific secondary ions. The exploitation of multi-ion emission events has both practical and fundamental applications. For instance, in the case of structural characterization one could look for correlations between fragment secondary ions emitted within these types of events. This information may provide some insight into how the surface structure affects the emission and fragmentation of secondary ions. From a practical standpoint these types of events maximize the amount of chemical and physical information from nano-domains thus increasing the sensitivity over more conventional SIMS measurements.

REFERENCES

[1] Chandra S, Lorey DR, Smith DR, Miura M, Morrison GH. *In Proceedings of the 12th International Conference on Secondary Ion Mass Spectrometry*, Brussels, 5-10 September 1999. Elsevier: Amsterdam, 2000; 927.

[2] Rollion-Bard C, Chaussidon M, France-Lanord C, Bard E. *In Proceedings of the 12th International Conference on Secondary Ion Mass Spectrometry*, Brussels, 5-10 September 1999. Elsevier: Amsterdam, 2000; 1015.

[3] Peterson RE, Tyler BJ. *In Proceedings of the 12th International Conference on Secondary Ion Mass Spectrometry*, Brussels, 5-10 September 1999. Elsevier: Amsterdam, 2000; 985.

[4] Kovarsky AP, Nikolaev AE, Jagovkina MA. *In Proceedings of the 12th International Conference on Secondary Ion Mass Spectrometry*, Brussels, 5-10 September 1999. Elsevier: Amsterdam, 2000; 677.

[5] English RD, Van Stipdonk MJ, Schweikert EA. *In Proceedings of the 12th International Conference on Secondary Ion Mass Spectrometry*, Brussels, 5-10 September 1999. Elsevier: Amsterdam, 2000; 809.

[6] Briggs D, Bryan SR. *In Proceedings of the 12th International Conference on Secondary Ion Mass Spectrometry*, Brussels, 5-10 September 1999. Elsevier: Amsterdam, 2000; 875.

[7] Krane KS. *Introductory Nuclear Physics.* John Wiley & Sons: New York, 1988.

[8] Wien K. *Lect. Notes Phys.* 1986; **269**: 1.

[9] Macfarlane RD. *Anal. Chem.* 1983; **55**: 1247A.

[10] Sundqvist R, Macfarlane RD. *Mass Spectrom. Rev.* 1985; **4**: 421.

[11] Knoll GF. *Radiation Detection and Measurement (2 edn)*. Wiley: New York 1989.

[12] Blain MG, Della-Negra S, Joret H, Le Beyec Y, Schweikert EA. *Phys. Rev. Lett.* 1989; **63:** 1625.

[13] Park MA, Cox BD, Schweikert EA. *J. Chem. Phys.* 1992; **96**: 8171.

[14] Van Stipdonk MJ, Park MA, Schweikert EA. *J. Mass Spectrom*. 1997; **32**: 1151.

[15] Park MA, Gibson KA, Quinones L, Schweikert EA. *Science* 1990; **248**: 988.

[16] Verkhoturov SV, Schweikert EA, Rizkalla NM. *Langmuir* 2002; **18**: 8836.

[17] Verkhoturov SV, Schweikert EA. *Anal. Bioanal. Chem.* 2002; **373**: 55.

[18] Van Stipdonk MJ, Schweikert EA. *Nucl. Instr. and Meth. B* 1994; **88**: 55.

[19] Keating CD, Natan NJ. *Adv. Mater.* 2003; **15**: 451.

[20] Reiss BD, Freeman RG, Walton ID, Norton SM, Smith PC, Stonas WG, Keating CD, Natan MJ. *Electroanal. Chem.* 2002; **522**: 95.

[21] Martin BR, Dermody DJ, Reiss BD, Fang M, Lyon LA, Natan MJ, Mallouk TE. *Adv. Mater.* 1999; **11**: 1021.

[22] Murray CB, Kagan CR, Bawendi MG. *Annu. Rev. Mater. Sci.* 2000; **30**: 545.

[23] Sra AD, Schaak RE. *J. Am. Chem. Soc.* 2004; **126**: 6667.

[24] Clearfield A. *Ann. Rev. Mater. Sci.* 1984; **14**: 205.

[25] Van Stipdonk MJ, Park MA, Schweikert EA, Sylvester P, Clearfield A. *Int. J. Mass Spectrom. Ion Processes* 1993; **128**: 133.

[26] Van Stipdonk MJ, Shapiro JB, Schweikert EA. *Vacuum* 1995; **46**: 1227.

[27] Rickman RD. PhD Dissertation, Texas A&M University, 2004.

[28] English RD, Van Stiponk MJ, Sabapathy RC, Crooks RM, Schweikert EA. *Anal. Chem.* 2000; **72**: 5973.

[29] Benguerba M, Brunelle A, Delle-Negra S, Depauw J, Joret H, Le Beyec Y, Blain MG, Schweikert EA, Ben Assayag G, Sudraud P. *Nucl. Instr. and Method in Phys. Res.* B 1991; **62**: 8.

[30] Rickman RD, Verkhoturov SV, Parilis ES, Schweikert EA. *Phys. Rev. Lett.* 2004; **92**: 47601.

[31] Bennett JA, Schweikert EA, Poisson D, Joliceur C. *Surf. Int. Anal.* 1990; **15**: 651.

[32] Park MA, Gibson KA, Quinones L, Schweikert EA. *Science* 1990; **248**: 988.

VITA

Sara Balderas was born to Jose Concepcion and Sara Balderas in Del Rio, Texas on June 5, 1977. She was reared by her guardians William Lee and Marie Victoria Humberd. She graduated from Del Rio High School in Del Rio, Texas in May of 1996. In September of 1996, she began college at Texas A&M University, College Station, TX. Sara received her B.S. degree in chemistry in May of 2001. During the summer of 1995, she worked as a research associate in Dr. Emile A. Schweikert's laboratory at Texas A&M University. In August of that same year, she enrolled at Texas A&M University to pursue a M.S. degree in chemistry under the guidance of Dr. Schweikert.

Her permanent address is that of her guardians:

202 North Orbit Street

Del Rio, Texas 78840